Energy-twisted boundary condition and response in one-dimensional quantum many-body systems

Ryota Nakai,[1,*] Taozhi Guo,[2,*] and Shinsei Ryu[2]
[1]*Department of Physics, Kyushu University, Fukuoka, 819-0395, Japan*
[2]*Department of Physics, Princeton University, Princeton, New Jersey, 08540, USA*

(Received 15 July 2022; accepted 28 September 2022; published 17 October 2022)

Thermal transport in condensed matter systems is traditionally formulated as a response to a background gravitational field. In this work, we seek a twisted-boundary-condition formalism for thermal transport in analogy to the U(1) twisted boundary condition for electrical transport. Specifically, using the transfer matrix formalism, we introduce what we call the energy-twisted boundary condition, and study the response of the system to the boundary condition. As specific examples, we obtain the thermal Meissner stiffness of (1+1)-dimensional CFT, the Ising model, and disordered fermion models. We also identify the boost deformation of integrable systems as a bulk counterpart of the energy-twisted boundary condition. We show that the boost deformation of the free fermion chain can be solved explicitly by solving the inviscid Burgers equation. We also discuss the boost deformation of the XXZ model, and its nonlinear thermal Drude weights, by studying the boost-deformed Bethe ansatz equations.

DOI: 10.1103/PhysRevB.106.155128

I. INTRODUCTION

Condensed matter systems are characterized by their responses to various background fields. For example, electrical conductivity is a (linear) response to an applied electric field. More formally, the system can be gauged or coupled to arbitrary background U(1) gauge field, and one can study the response of the system.

The electrical response is far from the complete characterization of the system. In particular, for charge-neutral systems or particle number nonconserving systems, we need to seek other responses. For example, thermal transport can be well-defined and investigated for generic systems. Luttinger [1] identified the gravitational field (gravitoelectric field) as a proper static background field to formulate the linear response for thermal transport. (This is based on the Tolman-Ehrenfest effect, which is similar to the Unruh effect.) This formalism allows us to study thermal transport in much the same way as electrical transport.

In this paper, we will further pursue parallelism between thermal and electrical response. In particular, we seek an analog of the twisted-boundary-condition formalism a la Kohn and Thouless [2–4]. In this approach, the system's sensitivity to the twisted boundary condition—the boundary condition twisted by the particle number conserving U(1) phase rotation—is related to the electrical transport. In this paper, we will discuss the boundary condition twisted by energy, which we call the energy-twisted boundary condition. Following the analogy, the sensitivity of the system to the energy-twisted boundary condition is expected to capture the system's transport properties.

For the case of electrical transport, twisting the boundary condition by U(1) phase is gauge equivalent to introducing bulk background U(1) gauge field. In particular, the bulk U(1) gauge field can be completely uniform (homogeneous). Similarly, in relativistic theories, the energy-twisted boundary condition can be thought of as a change in the background metric—we introduce the background graviphoton field [5,6]. This is equivalent to put the system in an accelerated frame. However, our formalism, the energy-twisted boundary condition, can be applied to any lattice quantum many-body systems, as far as energy is conserved—we can "accelerate" or "boost" lattice quantum many-body systems by using the energy-twisted boundary condition.

While the equivalence between the energy-twisted boundary condition and the bulk background metric may not hold for lattice quantum many-body systems in general, we will discuss an analog of the bulk formulation for the case of integrable lattice quantum many-body systems. Concretely, we will discuss the so-called boost deformation for integrable lattice quantum many-body systems.

In this paper, we will be mostly interested in (1+1)D systems, defined on a spatial circle (ring). The twisted boundary condition, twisted either by U(1) or by energy, can be thought of as arising from magnetic or gravitomagnetic flux threading through the ring. For the case of U(1), this is the setting where we can discuss persistent electrical current [7], related to the Aharonov-Bohm effect. With energy-twisted boundary condition, we can also discuss a gravitational analog of persistent current. Just like the persistent current is based on the Aharonov-Bohm effect, the thermal/gravitational analog can be thought of as related to the Sagnac effect [8]. The Aharonov-Bohm effect and the persistent current is periodic in the unit of flux quantum. When the threaded flux is an integer multiple of the flux quantum, the Hamiltonian is equivalent to the Hamiltonian without magnetic flux, as one can find a

[*]These authors contributed equally to this work.

large gauge (unitary) transformation which brings one into the other. While it is rarely discussed, there is a similar periodicity for the Sagnac effect, and for the gravitational persistent current. It is related to the large diffeomorphism (modular transformation) of the space-time torus.

The rest of the paper is organized as follows. In Sec. II, we first recall the twisted boundary condition by U(1) phase and its relation to the Drude weight and Meissner stiffness. Subsequently, we consider the generalization, the boundary condition twisted by time-translation symmetry. We then introduce the thermal version of the Drude weight and Meissner stiffness. The precise prescription for the energy-twisted boundary condition is discussed by using the tensor network representation of the transfer matrices. In addition, one can formulate the bulk perspective using the so-called boost deformation in integrable systems. In Sec. III, we present the calculation of the Meissner stiffness for (1+1)D CFT and for the transverse-field Ising model. In Appendix C, we also present the calculation of the Meissner stiffness for (1+1)D disordered free fermion models by using the transfer matrix method. In Sec. IV, we take a closer look at the integrable boost deformation, by first focusing on the free fermion chain. We will show that the boost deformation can be solved in terms of the inviscid Burgers equation. We also study the boost deformation for the XXZ model, and its thermal response, in particular, the nonlinear thermal Drude weights. Finally, we conclude in Sec. V.

II. ENERGY-TWISTED BOUNDARY CONDITION

A. U(1) twisted boundary condition, persistent current, Drude weight, and Meissner stiffness

Any symmetry in quantum field theories can be twisted. This is so in particular for unitary on-site symmetries. By twisting, we here mean twisting boundary conditions by symmetries. (One can also introduce symmetry twist defects, which are closely related.) Of interest to us in this paper is twisting by time translation symmetry (energy). Before discussing twisting by energy, let us start, as a warm-up, with a more familiar example of twisting by continuous U(1) symmetry.

To be specific, let us consider a lattice fermion system defined on a finite one-dimensional lattice of length L with the periodic boundary condition (PBC). That is, the system is defined on a spatial ring or circle. (The following discussion can easily be extended to systems defined on a d-dimensional spatial torus.) We use $\psi_i(x)$ to denote a fermion annihilation operator located at a site x, i represents some internal degrees of freedom within unit cell (spin, orbitals, etc.). For general systems, the boundary condition can be twisted, i.e., we can consider a twisting boundary condition, $\psi_i(x+L) = e^{i\varphi}\psi_i(x)$, where φ is a twisting phase (notice, however, that we have systems with conserved particle number in mind in the following to discuss conduction properties.) By using the generator of U(1), i.e., the total charge (total fermion number operator), $Q = \sum_x \sum_i \psi_i^\dagger(x)\psi_i(x)$, this boundary condition can be written as

$$\psi_i(x+L) = G_\varphi\, \psi_i(x)\, G_\varphi^{-1}, \quad G_\varphi = e^{i\varphi Q}. \tag{1}$$

As is well known, such twisting boundary condition can be realized by the Aharanov-Bohm effect, i.e., by putting magnetic flux through a nontrivial cycle of the circle. Such a magnetic flux may be introduced by a constant background gauge potential, e.g., $A(x) = \varphi/L$. This gauge potential enters into the hopping elements: $\psi_j^\dagger(x+1)e^{i\varphi/L}\psi_i(x) + \text{H.c.}$ By a gauge transformation $\psi_i(x) \to e^{i\varphi x/L}\psi_i(x)$, one can remove the background vector potential, $\psi_j^\dagger(x+1)e^{i\varphi/L}\psi_i(x) \to \psi_j^\dagger(x+1)\psi_i(x)$, except at the boundary of the system: $\psi_j^\dagger(1)e^{i\varphi/L}\psi_i(L) \to \psi_j^\dagger(1)e^{i\varphi}\psi_i(L) = \psi_j^\dagger(1)G_\varphi\psi_i(L)G_\varphi^{-1}$. After this gauge transformation, only the link connecting the ends at $x = 1$ and $x = L$ has a phase factor $e^{i\varphi}$.

The twisted boundary condition (1) can immediately be generalized to any unitary on-site symmetries by simply replacing G_φ by the unitary operator implementing the symmetry. It can also be generalized to non-on-site symmetries [9], and to antiunitary symmetries (time-reversal symmetry) [9,10]. These twisting are useful, e.g., to detect symmetry-protected topological phases.

With the twisted boundary condition, we can now discuss the system's response to the U(1) twist, and associated quantities that measure the response [2,11–15]. (Here, we follow the notation of Ref. [14].) First, when the boundary condition is twisted by a U(1) phase, $\psi_i(x+L) = e^{i\varphi}\psi_i(x)$, inversion symmetry is broken and a finite electric current, the persistent current,

$$J = L\frac{dF}{d\varphi} = L\sum_n \frac{e^{-\beta E_n}}{Z}\frac{dE_n}{d\varphi}, \tag{2}$$

flows in the ground state, where $E_n(\varphi)$ is the many-body eigenenergy as a function of the twisted U(1) phase, $Z = \sum_n e^{-\beta E_n}$ is the partition function, and $F = -\beta^{-1}\ln Z$ is the free energy. By taking the second derivative with respect to the U(1) phase φ, we can measure the stiffness of a system against the U(1) twist. There are two similar but different quantities, the Drude weight (charge stiffness) $\bar{D}$ and the Meissner stiffness D. They are defined, respectively, by

$$\bar{D} = \frac{L}{2}\sum_n \frac{e^{-\beta E_n}}{Z}\frac{d^2E_n}{d\varphi^2}\bigg|_{\varphi=0}, \tag{3}$$

$$D = \frac{L}{2}\frac{d^2F}{d\varphi^2}\bigg|_{\varphi=0}. \tag{4}$$

In transport theory of free fermions, the Drude weight describes the singular part of the ac electric conductivity $\sigma(\omega)$ at zero frequency $\omega = 0$,

$$\mathrm{Re}\,\sigma(\omega) = 2\pi\bar{D}\delta(\omega) + \sigma_{\mathrm{reg}}(\omega). \tag{5}$$

On the other hand, the Meissner stiffness measures the superfluid density and describes the boundary-U(1)-phase dependent part of the ac conductivity as

$$\sigma(\omega) = \frac{2iD}{\omega + i\delta} + \sigma_{\mathrm{KG}}(\omega). \tag{6}$$

The second term of the right-hand side is the Kubo-Greenwood formula of the ac conductivity

In the limit of $L \to \infty$ and then $T \to 0$, the Drude weight is a measure of metallicity [2], and the Meissner stiffness

is that of superconductivity [12], that is, $D = \bar{D} = 0$ in insulators, $D = 0, \bar{D} = 0$ in metals, and $D = \bar{D} = 0$ in superconductors. The coincidence of the two stiffnesses occurs when the energy gap is present [12]. In the limit of $L \to \infty$ but at a finite temperature, D is a measure of ballistic conduction or integrability [16–19], while $D = 0$ in one dimension. As for a finite-size system, there is typically an energy gap above the ground state. Thus, at $T \to 0$, the Drude weight and the Meissner stiffness coincide provided there is no ground state degeneracy [13].

B. Energy-twisted boundary condition

We shall now generalize the above line of thinking to time translation symmetry. Following (1), we are interested in the "energy-twisted" boundary condition,

$$\psi_i(x + L) = e^{aH}\psi_i(x)e^{-aH}, \tag{7}$$

where H is the Hamiltonian, and a is a parameter.

To give a precise meaning of (7), we can switch to the imaginary-time (Euclidean) path-integral language, where the energy-twisted boundary condition can be introduced, in term of the space-time field, as

$$\psi_i(x + L, \tau) = \psi_i(x, \tau + a), \tag{8}$$

where τ is the imaginary time. We should note that the imaginary time is periodic, with the periodicity given by the inverse temperature β, $\tau \equiv \tau + \beta$. Accordingly, while not apparent in (7), there is a periodicity in the twist parameter a with the periodicity, $a \equiv a + \beta$, much the same way as the U(1) twisted boundary condition is periodic with periodicity given by the flux quantum, $2\pi = 2\pi\hbar c/|q|$ where $\hbar = c = 1$ and we choose the charge of the matter field to be one, $|q| = 1$. We will call the boundary condition of type (7) or (8) as energy-twisted boundary condition. We will also work with the rescaled version of a,

$$\kappa = \frac{a}{L}, \tag{9}$$

in terms of which the periodicity condition is given by $\kappa \equiv \kappa + \beta/L$.

It is also useful to consider discretized imaginary time and the transfer matrix, as commonly done in lattice quantum many-body systems. The energy-twisted boundary condition can then be conveniently introduced when we have a matrix-product-operator representation of the (column-to-column) transfer matrix. If we discretize the imaginary-time direction into M lattice sites, $\beta = 1\tau \times M$, the partition function can be written in terms of the row-to-row transfer matrix $V \equiv e^{-1\tau H}$ as $Z = \mathrm{Tr}[V^M]$. When the system's transfer ma-trix is represented in terms of a matrix product operator, the partition function on the torus is then given in terms of a tensor network, as depicted in Fig. 1. The partition function can be alternatively written in terms of the column-to-column transfer matrix W,

$$Z = \mathrm{Tr}[V^M] = \mathrm{Tr}[W^L]. \tag{10}$$

Now, we distort this space-time lattice, and consider the partition function on the twisted torus (Fig. 1 right). This

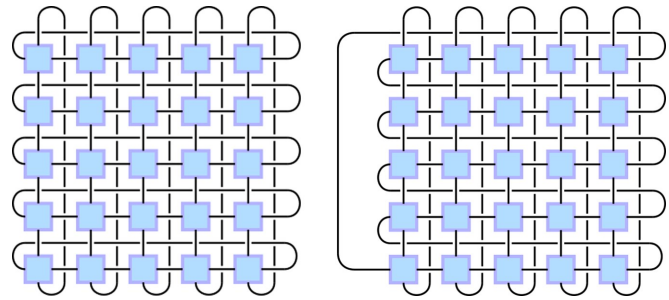

FIG. 1. The tensor network representation of the untwisted (left) and twisted (right) partition functions.

can be achieved by "reconnecting" the relevant links, located between $x = L$ and $x = 1$. This reconnection implements a discrete version of the energy-twisted boundary condition. We note that twisted *spatial* tori have been discussed in the context of topological order [20,21] and Lieb-Schultz-Mattis type theorems [22,23].

Viewing the horizontal direction as a fictitious time direction, this may be viewed as an insertion of an operator in the column-to-column picture

$$Z_{\mathrm{twist}}(a) = \mathrm{Tr}[W^L S^a], \tag{11}$$

where S is the unit shift operator in time direction, that shifts the temporal coordinate by 1τ. The twist parameter a here is an integer. We note when $a = M$, $S^M = \mathbf{1}$, and hence the twisted partition function is periodic in a, $Z_{\mathrm{twist}}(a + M) = Z_{\mathrm{twist}}(a)$.

C. Energy-twisted boundary condition and deformation in integrable systems

While the above prescription to introduce energy-twisted boundary condition is generic, we now turn our attention to integrable lattice systems and quantum field theories in (1+1) dimensions. There, the energy-twisted boundary condition can be implemented without breaking their integrability. Integrability of these models also allows us to consider their boost deformations—*bulk* deformations of the models without breaking integrability [24]. Boost deformation is to energy-twisted boundary condition what bulk U(1) gauge field is to U(1) twisted boundary condition. Namely, boost deformations provide a bulk background "gauge field" corresponding to the energy-twisted boundary condition.

Let us now briefly review the boost deformation in integrable (1+1)D lattice quantum many-body systems, by first using the set of conserved charges, and then by using the coordinate Bethe ansatz. The latter description makes its connection to the energy-twisted boundary condition clear, while in the former we have a bulk description in terms of a deformed Hamiltonian.

We recall that integrable spin chains come with an infinite tower of commuting charges $\{Q_r\}$, $[Q_r, Q_s] = 0$ $(r, s = 2, 3, \ldots)$, the existence of which is the manifestation of the integrability. Among the conserved charges is the Hamiltonian of the spin chain, $H = Q_2$. Ref. [24] introduced one parameter deformations of generic integrable quantum spin chains. Starting from the infinite tower of commuting charges

$\{Q_r\}$ of the original short-range spin chain, the scheme introduced in Ref. [24] continuously deforms the conserved charges $\{Q_r\} \to \{Q_r(\lambda)\}$ where λ is the deformation parameter. Under such deformation, the integrability is maintained, i.e., $[Q_r(\lambda), Q_s(\lambda)] = 0$, but the deformed charges are longer-ranged. One of the examples of the deformations is the so-called $T\bar{T}$ deformation [25]. Of our interest here is the boost deformation, which is defined, for the second conserved charge (the Hamiltonian), by

$$\frac{dQ_r(\lambda)}{d\lambda} = i[B[Q_2(\lambda)], Q_r(\lambda)]. \tag{12}$$

Here, $B[Q_2(\lambda)]$ is the boost operator for the charge Q_2 and defined by

$$B[Q_2] = \sum_x x\, q_2(x), \tag{13}$$

where $q_2(x)$ is the density of Q_2, $Q_2 = \sum_x q_2(x)$. The boost-deformed Hamiltonian $Q_2(\lambda) = H(\lambda)$ is an analog of the Hamiltonian $H(\varphi)$ in the presence of background U(1) gauge field $A(x) = \varphi/L$ discussed in Sec. II A. As will be seen in Eq. (30), the parameter λ can be identified with the parameter a, κ introduced in Sec. II as

$$i\lambda = \kappa, \tag{14}$$

i.e., an analytic continuation of κ. We note that the flow equation (12) for real λ keeps the conserved charges hermitian, while the operator twisting the boundary condition in (7) is nonunitary when a and κ are real.

In the above, the boost deformation is conveniently described for infinite systems. It is however possible to discuss integrability and the deformation for finite chains. There, we need to worry about the compatibility between the long-range nature of the deformed conserved charges, and the finite size of the system with a boundary condition. As long as the range of a conserved charge of interest does not exceed the length of the chain L, one can formulate the Bethe ansatz equations, and expect that they give the correct spectrum for this particular charge. The Bethe ansatz equations we use here are asymptotic ones, valid for large enough L.

Let us consider, as an example, the $S = 1/2$ XXZ spin chain

$$H = J \sum_{x=1}^{L} \left[S_x^x S_{x+1}^x + S_x^y S_{x+1}^y + \Delta S_x^z S_{x+1}^z \right] - \frac{LJ\Delta}{2}. \tag{15}$$

In the following, we will assume L to be even, and $J > 0$ and $-1 < \Delta < 1$. We parametrize the anisotropy Δ as $\Delta = \cos\gamma$. The coordinate Bethe ansatz for a state containing N "particles" with (quasi) momenta $p_1, \ldots, p_N$ is given by

$$|v_N\rangle = \sum_{x_1<x_2<\cdots<x_N} \sum_{\sigma\in S_N} \prod_{j>k} f(v_{\sigma_j} - v_{\sigma_k}) \times \prod_{j=1}^{N} e^{ip_{\sigma_j}x_j} S_{x_1}^- \cdots S_{x_N}^- |\uparrow\cdots\uparrow\rangle, \tag{16}$$

where S_N is the symmetric group of degree N and $S_{x_j}^- = S_{x_j}^x - iS_{x_j}^y$. Here, we introduce the rapidity variable v_j,

$$e^{ip_j} = e^{ip(v_j)} = \frac{\sinh\frac{\gamma}{2}(v_j + i)}{\sinh\frac{\gamma}{2}(v_j - i)}, \tag{17}$$

and $f(v)$ is related to the S matrix and the phase shift,

$$S(v) = e^{i\delta(v)} = -\frac{\sinh\frac{\gamma}{2}(v + 2i)}{\sinh\frac{\gamma}{2}(v - 2i)}, \tag{18}$$

by $S(v) = f(v)/f(-v)$. The energy for the state (16) is given by

$$E = \sum_{j=1}^{N} h(v_j) = \sum_{j=1}^{N} \frac{2J\sin^2\gamma}{\cos\gamma - \cosh(\gamma v_j)}. \tag{19}$$

Requiring PBC, we obtain the Bethe ansatz equations

$$e^{ip(v_j)L} = \prod_{k(\neq j)} S(v_j - v_k), \quad j = 1, \ldots, N, \tag{20}$$

that determine the quasi momenta.

The boost deformation results in the change in momentum $p(v_j) \to p_\lambda(v_j)$ [24]. We can then consider the modified Bethe ansatz equations

$$e^{ip_\lambda(v_j)L} = \prod_{k(\neq j)} S(v_j - v_k). \tag{21}$$

As mentioned above, these Bethe ansatz equations are asymptotic ones, valid for large enough L. In Ref. [26], it was shown that, in infinite volume, the deformed momentum p_λ depends linearly on λ,

$$p_\lambda(v_j) = p_{\lambda=0}(v_j) + \lambda h(v_j), \tag{22}$$

which is an input to the Bethe ansatz equations.

D. Thermal response

In analogy to the U(1) case, we expect that the energy-twisted boundary condition and deformation (12) is related to thermal transport. The commutator of the Hamiltonian with the boost operator [the right-hand side of (12) when $r = 2$] is the energy current operator, which is an integral of motion in integrable models. The persistent heat current (an analog of the persistent charge current) flowing in the ground state of a boost-deformed Hamiltonian is thus

$$J^Q = -\left\langle \frac{dQ_2}{d\lambda} \right\rangle = -\sum_n \frac{e^{-\beta E_n}}{Z} \frac{dE_n}{d\lambda} = -\frac{dF}{d\lambda}. \tag{23}$$

From the linear response theory, we can define the thermal Drude weight [14], which is the zero-frequency singularity part of the ac thermal conductivity

$$\mathrm{Re}\,\kappa(\omega) = \frac{2\pi\bar{D}^Q}{T}\delta(\omega) + \kappa_{\mathrm{reg}}(\omega), \tag{24}$$

and the thermal version of the Meissner stiffness [14], which is the contribution to the thermal conductivity besides the Kubo-Greenwood part [1]

$$\kappa(\omega) = \frac{2iD^Q}{T(\omega + i\delta)} + \kappa_{\mathrm{KG}}(\omega). \tag{25}$$

Notice that the definition of these quantities is due to Ref. [14], which may be different from other references by T and a constant. As expected, the thermal Drude weight and Meissner stiffness of free fermions are identified with the second derivatives of the energy and free energy, respectively, with respect to the boost-deformation parameter λ as

$$\bar{D}^Q = \frac{1}{2L}\sum_n \frac{e^{-\beta E_n}}{Z}\frac{d^2E_n}{d\lambda^2}\bigg|_{\lambda=0}, \tag{26}$$

$$D^Q = \frac{1}{2L}\frac{d^2F}{d\lambda^2}\bigg|_{\lambda=0}. \tag{27}$$

(see Appendix D).

At a finite temperature, the thermal Meissner stiffness is zero unless superconducting [14]. The thermal Drude weight has been studied in 1d quantum systems in [27–32]. [Specifically, see (43).]

III. ENERGY-TWISTED BOUNDARY CONDITION AND THERMAL MEISSNER STIFFNESS

In this section, we consider the energy-twisted boundary condition in (1+1)D CFT and lattice many-body systems, and calculate the thermal Meissner stiffness.

A. (1+1)D CFT

Let us start with a simple example, the (1+1)D chiral Dirac fermion theory,

$$H = \int_0^L dx\, \psi^\dagger H \psi, \quad H = -iv\partial_x, \tag{28}$$

where $\psi(x)$ is a complex fermion field operator, and v is the Fermi velocity. The single-particle eigen functions are given by $f_p(x) = e^{ipx}/\sqrt{L}$ with the single-particle energy $\varepsilon(p) = vp$, $Hf_p(x) = \varepsilon(p)f_p(x)$. Requiring the regular (unboosted) PBC leads to the quantization of p, $p = 2\pi/L \times$ *integer*. The energy-twisted boundary condition can be imposed by requiring

$$f_p(x+L) = e^{ipL}f_p(x) = e^{\kappa\varepsilon(p)L}f_p(x), \tag{29}$$

where κ is the twist parameter. Thus, p is quantized as

$$(p + i\kappa\varepsilon(p))L = 2\pi n, \quad n \in \mathbf{Z},$$
$$\Rightarrow p = \frac{1}{1+iv\kappa}\frac{2\pi n}{L}. \tag{30}$$

This equation should be compared with (21) with $i\lambda = \kappa$.

We now consider the partition function in the presence of energy-twisted boundary condition. In relativistic systems this can be incorporated by introducing graviphoton field in the background metric (Appendix A). For 2-torus, the twist can be incorporated by modifying the modulus. For the untwisted case, the partition function is

$$Z = \mathrm{Tr}\, e^{-\beta H} = \mathrm{Tr}\, q^{L_0 - c/24}, \tag{31}$$

where L_0 is the Virasoro generator, $c = 1$ is the central charge, and q is given by

$$q = e^{2\pi i\tau} = e^{-\frac{2\pi v\beta}{L}}. \tag{32}$$

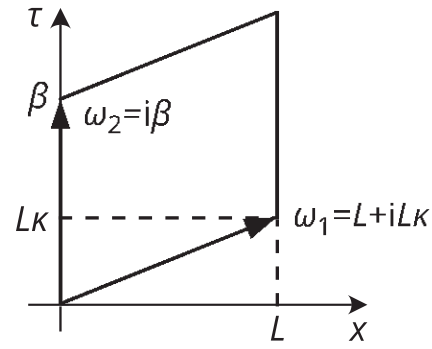

FIG. 2. The space-time torus with the energy-twisted boundary condition. (Here, we set the velocity to be one, $v = 1$, for simplicity.)

With (30), the partition function in the presence of the twist is given by $Z = \mathrm{Tr}\, q^{L_0 - c/24}$, where q is now given by

$$q = e^{2\pi i\tau} = e^{-\frac{2\pi v\beta}{L}\frac{1}{1+iv\kappa}}. \tag{33}$$

Namely, the modulus changes from the untwisted to twisted case as

$$\tau = \frac{iv\beta}{L} \to \frac{iv\beta}{L}\frac{1}{1+iv\kappa}. \tag{34}$$

Recall that the modulus is the ratio of two periodicities ω_1 and ω_2 on the complex plane, $\tau = \omega_2/\omega_1$. After the twist, ω_1 is changed as $L \to L + iLv\kappa$, while $\omega_2 = iv\beta$ remains unchanged (Fig. 2). When $\kappa = \beta/L$, (34) is nothing but the modular transformation TST,

$$\tau \to \frac{\tau}{1+\tau}, \tag{35}$$

where $T : \tau \to \tau + 1$ and $S : \tau \to -1/\tau$ are the genera-tors of the modular group $SL(2, \mathbf{Z})/\mathbf{Z}_2$: $\tau \to (a\tau + b)/(c\tau + d)$ $(a, b, c, d \in \mathbf{Z})$. The modular transformation leaves the space-time torus unchanged (it acts as a large diffeomorphism), and hence the space-time at κ and $\kappa + \beta/L$ are equivalent.

Let us now consider the energy-twisted boundary condition in a generic (1+1)D CFT using the formalism in Sec. II. In Lorentz invariant theories, row-to-row and column-to-column transfer matrices are essentially the same. The row-to-row transfer matrix is given in terms of the Hamiltonian H as $V = \exp(-H)$. For a CFT placed on the spatial circle of circumference L, H is given in terms of the Virasoro generators L_0 and $\bar{L}_0$ and the central charge c as $H = (2\pi v/L)(L_0 + \bar{L}_0 - c/12)$. ($v$ is the velocity of the excitations and plays the role of the speed of light.) The corresponding column-to-column transfer matrix is given by $W = \exp(-\tilde{H})$ where $\tilde{H} = (2\pi/v\beta)(L_0 + \bar{L}_0 - c/12)$. The partition function can be written in two different ways, $Z(\beta, L) = \mathrm{Tr}_H\, e^{-\beta H} = \mathrm{Tr}_{\tilde{H}}\, e^{-L\tilde{H}}$, where H and $\tilde{H}$ are the CFT Hilbert space on a ring of circumference L and β, respectively. Introducing the moduli as

$$\tau = iv\beta/L, \quad \bar{\tau} = -iv\beta/L,$$
$$\tilde{\tau} = -1/\tau, \quad \bar{\tilde{\tau}} = -1/\bar{\tau}, \tag{36}$$

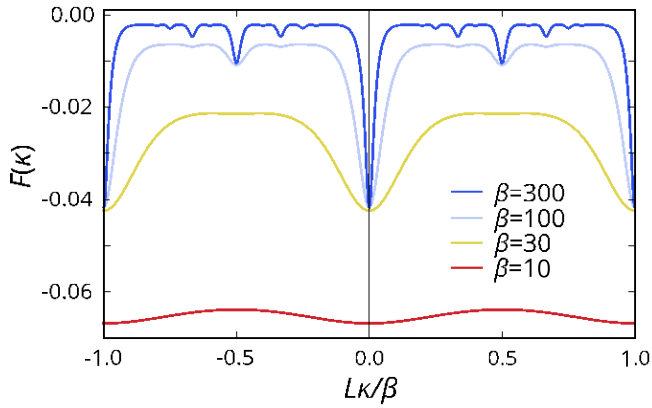

FIG. 3. The variation of the free energy of the Ising CFT with energy twist.

the partition function can be written as

$$Z(\beta, L) = \mathrm{Tr}_H\, e^{2\pi i\tau(L_0-c/24)}e^{-2\pi i\bar{\tau}(\bar{L}_0-c/24)} = \mathrm{Tr}_{\tilde{H}}\, e^{2\pi i\tilde{\tau}(L_0-c/24)}e^{-2\pi i\bar{\tilde{\tau}}(\bar{L}_0-c/24)}. \quad (37)$$

To introduce the energy twist, we modify the moduli as

$$\tau = \frac{iv\beta}{L} \to \frac{iv\beta}{L}\frac{1}{1+iv\kappa}, \qquad \tilde{\tau} = \frac{iL}{v\beta} \to \frac{iL}{v\beta}(1+iv\kappa). \quad (38)$$

The energy-twisted partition function is invariant under $\tilde{\tau} \to \tilde{\tau}+n$ or $L\kappa \to L\kappa + n\beta$, where n is an integer.

The energy-twisted partition function in the low-temperature limit, $v\beta/L \to \infty$, can be evaluated as

$$Z(\beta, L) \simeq e^{2\pi i\tau(h-\frac{c}{24})}e^{-2\pi i\bar{\tau}(h-\frac{c}{24})}, \quad (-1/\beta)\ln Z \simeq -\frac{(c-24h)\pi v}{6L(1+v^2\kappa^2)} \quad (39)$$

Here, h denotes the (rescaled) ground state energy. The thermal Meissner stiffness in the low-temperature limit converges to

$$D^Q(T=0) \simeq -\frac{(c-24h)\pi v^3}{6L^2}. \quad (40)$$

This quantifies the variation of the ground state energy in response to the energy-twisted boundary condition. According to Appendix D 1, $D^Q(T=0)$ agrees with the same limit of the thermal Drude weight $\bar{D}^Q(T=0)$ due to the presence of a finite-size gap and the uniqueness of the ground state. As an example, the twisted free energy of the Ising CFT is plotted in Fig. 3. The behavior near $\kappa = 0$ matches with (39) with $h = 0$.

Between $L\kappa/\beta = 0$ and 1, the free energy at low temperature has smaller Lorentzian peaks

$$F' \sim -\frac{(c-24h)\pi v}{6q^2L(1+v^2\delta\kappa^2)}, \quad (41)$$

at $L\kappa/\beta = p/q + L\delta\kappa/\beta$, where p and q are mutually coprime integers and $\delta\kappa$ is a small deviation from p/q (see Fig. 3). Specifically, a peak at $L\kappa/\beta = 1/2$ is 1/4 the height at $\kappa = 0$, peaks at $L\kappa/\beta = 1/3$ and 2/3 are 1/9 the height at $\kappa = 0$, and so on. These peaks have the same origin as the fidelity after a quantum quench in CFT [33]. The quench dynamics at a time t are traced by a modulus $\tau = v(i\beta + t)/L$, which is related to our twist by the S-modular transformation and interchanging β and L. As a result, the fidelity has more peaks at higher temperature, while the energy-twisted free energy has more peaks at lower temperature.

Following [33], the formula (41) can be derived as follows. A successive application of modular transformations $ST^{n_0}ST^{n_1}\cdots ST^{n_k}$ maps a modulus $\tau = q/p$ to $\tau = 0$, where $n_0, \cdots, n_k$ are integers appearing in the continued fraction of p/q as

$$\frac{p}{q} = n_0 - \cfrac{1}{n_1 - \cfrac{1}{n_2 - \cdots}}. \quad (42)$$

By the same modular transformation, a modulus $\tau = iv\beta/(L + iv(p/q)\beta + ivL\delta\kappa)$ is mapped to $\tau' \sim iq^2L(1+iv\delta\kappa)/v\beta$ when $v\beta/L \gg 1$, which relates the behavior around $L\kappa/\beta = p/q$ with that around $\kappa = 0$. Finally performing the S transformation again, the free energy (41) is obtained, provided $v\beta/L \gg q^2$ and $L\delta\kappa \ll \beta$.

On the other hand, high-temperature ($v\beta/L \ll 1$) behavior can be addressed provided the modular invariance is present. From (37), we obtain $D^Q \simeq 0$, which agrees with [14]. Notice that high temperature in CFT indicates a temperature regime that is much higher than the energy-level spacing. At high temperature in CFT but, simultaneously, sufficiently lower than other energy scales, such as the band width or Ising coupling, the thermal Drude weight estimated from the heat current has been reported [29,31], and is given by

$$\bar{D}^Q = \frac{(c-24h)\pi v T^2}{6}. \quad (43)$$

B. The transverse-field Ising model

While in the above we demonstrated the basic ideas using (1+1)D CFT as an example, it is interesting to apply the idea to broader systems, which do not have conformal symmetry nor Lorentz invariance. Here, we consider the transverse-field Ising model

$$H = \sum_{i=1}^{L}\left(-J\sigma_i^x\sigma_{i+1}^x - h\sigma_i^z\right), \quad (44)$$

satisfying PBC ($\sigma_{L+1} = \sigma_1$). The Ising coupling favors a ferromagnetically ordered phase ($J > h$), and the transverse field favors a disordered (paramagnetic) phase ($J < h$). These phases are related to each other by an order-disorder duality transformation [34]. The phase transition between them occurs at $h/J = 1$ (the self-dual point), at which the low-energy properties are described by the Ising CFT [35].

We use the transfer matrix formalism introduced in Sec. II to calculate the response to the energy-twisted boundary condition. Some details can be found in Appendix B. The twisted free energy $F(\kappa) = -\beta^{-1}\ln Z(\kappa)$ is evaluated numerically for a ring of perimeter $L = 10$. Here, we fix the Ising coupling by $J = 1$. The free energy at the critical point ($h = J = 1$) agrees with the CFT result (Fig. 4 bottom left). The free energy has a period of $\kappa = \beta/L$ and the peaks of the free energy become clear as the temperature is lowered. The free energy changes nonmonotonically as a function of

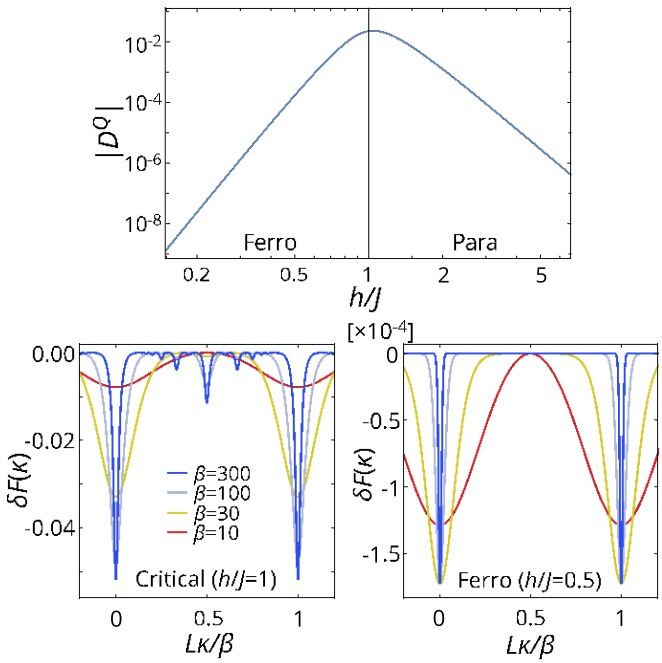

FIG. 4. (Top) The thermal Meissner stiffness of the transverse-field Ising model ($L = 10$ and $J = 1$) at $\beta = 100$. (Bottom) The variation of the free energy of the transverse Ising model at the critical point ($J = h = 1$, left) and in a ferromagnetic phase ($J = 1$, $h = 0.5$, right) and the perimeter $L = 10$ against the twist parameter κ is shown for temperature $\beta = 10$, 30, 100, and 300 (from red to blue).

the twist parameter κ, which is in stark contrast to a monotonically varying free energy of electrons under the U(1) twist within a single quantum flux, exhibiting a saw-tooth shape. The free energy shifted by a suitable constant is plotted.

Away from the critical point, we can see that the free energy variation decays rapidly due to the stiffness of the order (Fig. 4 bottom right). In addition, the free energy peaks besides $L\kappa/\beta =$ (integer) fade out even at low temperature. The peak height at these points is no longer related to that at the origin as it is at the critical point. This would be a signature of the deviation of the theory from the Ising CFT. The free energy profile obeys the duality of the model, that is, $h/J < 1$ in the ferromagnetic phase and $h^0/J_0 = (h/J)^{-1} > 1$ in the paramagnetic phase have the same response against the twist.

In Appendix C, we consider yet another lattice model, the 1d disordered free fermion model(s), and discuss the thermal Meissner stiffness.

IV. BOOST DEFORMATION IN INTEGRABLE SYSTEMS

In this section, we discuss the boost deformation in (1+1)D integrable lattice systems. In particular, we first look at the free fermion model in detail and show that the boost deformation leads to the Burgers equation of the single-particle dispersion. We then turn to the XXZ model, and, by using the boost-deformed Bethe ansatz equations, calculate the ground state energy as a function of the boost parameter, and the thermal Drude weight.

A. The free fermion model

The boost deformation and the inviscid Burgers equation. We start from the (undeformed) tight-binding model on a 1d lattice ($x \in \mathbf{Z}$), $H = -\sum_x (c_x^\dagger c_{x+1} + \text{H.c.})$, which defines the initial condition $Q_2(\lambda = 0) = H$ of the boost deformation (12). It is straightforward to verify that the Hamiltonian (the second charge) stays quadratic during the boost deformation. Hence, we represent the Hamiltonian and the corresponding boost operator as

$$Q_2(\lambda) = \sum_{x,z} t_z(\lambda) c_x^\dagger c_{x+z},$$
$$B[Q_2(\lambda)] = \sum_{x,z} (x + z/2) t_z(\lambda) c_x^\dagger c_{x+z}, \tag{45}$$

where the set of λ-dependent coefficients $t_z(\lambda)$ parameterize the boost-deformed Hamiltonian with the initial condition $t_z(\lambda = 0) = -\delta_{1,z} - \delta_{-1,z}$. In terms of the coefficients $t_z(\lambda)$, the flow equation of the boost deformation (12), reduces to

$$\frac{dt_z(\lambda)}{d\lambda} = -\frac{iz}{2} \sum_w t_w(\lambda) t_{z-w}(\lambda). \tag{46}$$

Starting from the nearest neighbor tight-binding model $Q_2(\lambda = 0)$, the boost deformation (12) [or the coupled ODE (46)] generates a longer-range hopping Hamiltonian $Q_2(\lambda)$. For a given λ, we consider a large enough chain of length L, and impose PBC. By the Fourier transform $c_x = L^{-1/2} \sum_k e^{ikx} \tilde{c}_k$, $[k = 2\pi(\text{integer})/L]$, the Hamiltonian in momentum space is $H(\lambda) = \sum_k f(\lambda, k) \tilde{c}_k^\dagger \tilde{c}_k$, where the energy dispersion $f(\lambda, k)$ is given by the Fourier transform of $t_z(\lambda)$:

$$f(\lambda, k) := \sum_w e^{iwk} t_w(\lambda). \tag{47}$$

From the perspective from the coupled ODE (46), the dispersion $f(\lambda, k)$ can be considered as the "generating function" of the coefficients $t_z(\lambda)$. So far as the generating function is differentiable with respect to k, it obeys a PDE, the inviscid Burgers equation

$$\frac{\partial f}{\partial \lambda} + f \frac{\partial f}{\partial k} = 0, \tag{48}$$

which can be derived from (46).

The inviscid Burgers equation has a formal solution derived by the method of characteristics [36]. The equienergy contour in the λ-k space is $k = \lambda f(\lambda = 0, k_0) + k_0$ that emanates from a point $(\lambda, k) = (0, k_0)$. This equation indicates how an initial state with a momentum k_0 and an eigenenergy $f(0, k_0)$ evolves by fixing the eigenenergy. A state of $(k, f(\lambda, k))$ on the dispersion relation moves along the momentum direction at a speed of $f(\lambda, k) = f(0, k_0)$. Thus the deformed dispersion relation is obtained by tilting the energy axis by $\arctan \lambda$. The Hamiltonian can be deformed until the dispersion relation becomes singular, where the slope of the dispersion relation diverges. Beyond this point, the generating function is no longer differentiable (the formation of the shock wave by the terminology of the hydrodynamics).

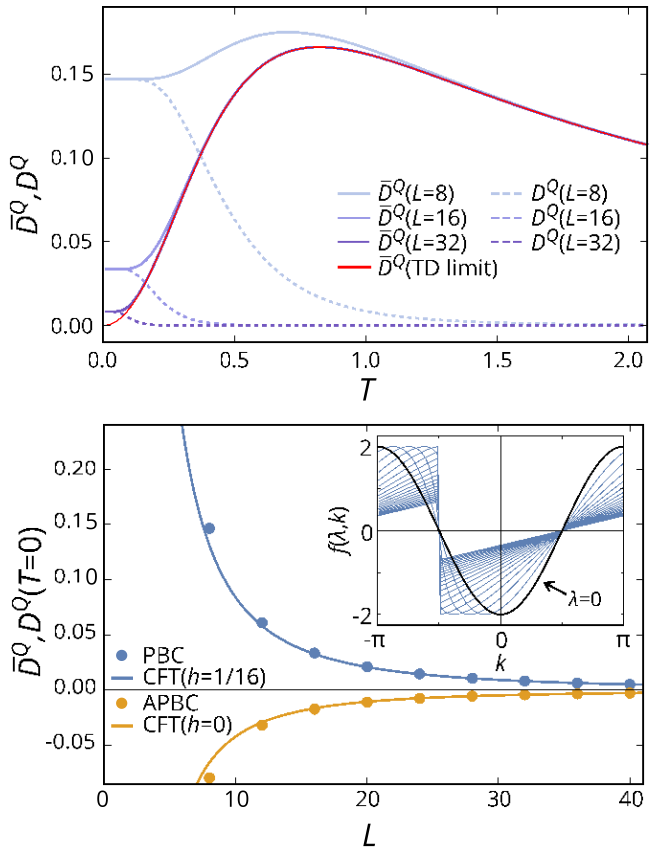

FIG. 5. (Top) The thermal Drude weight and thermal Meissner stiffness of the free fermion chain with $L = 8, 16, 32$ (solid and dotted lines, respectively) and the thermal Drude weight in the thermodynamic limit (red line). (Bottom) The thermal Drude weight (thermal Meissner stiffness) at zero temperature is shown. The inset is the evolution of the dispersion relation from $\lambda = 0$ (black) to $\lambda = 4$.

When the generating function is not differentiable with respect to k, it obeys an integro-differential equation

$$\frac{\partial}{\partial\lambda}\int dk\, e^{-iwk} f(\lambda,k) = \frac{1}{2}\int dk \frac{\partial e^{-iwk}}{\partial k} f(\lambda,k)^2. \tag{49}$$

Solutions to (49) are known as weak solutions to the inviscid Burgers equation (48). We should regard the weak solutions as the genuine generating function since the integro-differential equation (49) is equivalent to (46).

A nondifferentiable solution to the inviscid Burgers equa-tion can also be addressed by the inviscid limit of the Burgers equation, which is exactly solvable by the Cole-Hopf transformation. In general, the asymptotic solution of the Burgers equation in the inviscid limit becomes a linear dispersion $f(\lambda,k) = (k - k_M)/\lambda$, where k_M satisfies $f(0,k_M) = 0$ and $\partial f(0,k_M)/\partial k > 0$.

Specifically, the dispersion of the deformed Hamiltonian is the solution of

$$f(\lambda,k) = -2\cos[k - \lambda f(\lambda,k)]. \tag{50}$$

The evolution of the dispersion relation is shown in the inset of Fig. 5 (bottom). Starting from $f(0,k) = -2\cos k$, the shock wave is formed after $\lambda = 1/2$, where the slope at $k = -\pi/2$ diverges, and the dispersion relation converges to $f(\lambda,k) = (k - \pi/2)/\lambda$ ($k \in [-\pi/2, 3\pi/2]$).

The boost deformation, the thermal Drude weight, and the thermal Meissner stiffness. The thermal Drude weight and the thermal Meissner stiffness of the lattice free fermion model calculated by (26) and (27) are plotted in Fig. 5. As shown in Appendix D 3, the thermal Drude weight of a clean fermion system converges to $\pi v T^2/6$ in the thermodynamic limit $L \to \infty$ at low temperature $T \ll 1$. The thermal Drude weight (and thermal Meissner stiffness) at $T = 0$ is consistent with the CFT result (40) by taking into account that a complex fermion is equivalent to two real fermions ($c = 1/2$) and that $2(c - 24h) = -2$ for PBC ($h = 1/16$) and $2(c - 24h) = 1$ for APBC ($h = 0$). However, notice that physical properties of a free fermion depends on the length modulo 4 (for details see Appendix D 4).

B. The XXZ chain with boost deformation

We now turn to the boost deformation of the XXZ model (15). As outlined in Sec. II C, the boost deformation can be implemented in the Bethe ansatz equations. Specifically, we solve

$$L\left[p_1\left(v_j^\lambda\right) + \lambda h\left(v_j^\lambda\right)\right] - \sum_{k=1}^{N} p_2\left(v_j^\lambda - v_k^\lambda\right) = 2\pi I_j \tag{51}$$

with $p_n(v) = 2\tan^{-1}\left(\frac{\tanh\frac{\nu v}{2}}{\tan\frac{n\nu}{2}}\right)$. Here, focusing on the ground state at half-filling, $N = L/2$, the quantum numbers in (51) are given by $I_j = -\frac{N-1}{2} + j - 1$. We then obtain the ground state energy $E(\lambda)$ as a function of the boost parameter (Fig. 6).

When $\lambda = 0$, we have checked that the calculation using the boost-deformed Bethe ansatz equations reproduces the free fermion result. We observe that for small λ, there is a "plateaulike" structure, whereas for larger λ, the ground state energy depends more sensitively on λ. At the free fermion point $\lambda = 0$, this change in the behavior of the ground state energy coincides with the formation of the shock wave in the dispersion at $\lambda = \pm 1/2$.

The finite-size scaling of the zero temperature thermal Drude weight is shown in the bottom plot of Fig. 6. Here, as we take the limit $\beta \to \infty$ before $L \to \infty$, the thermal Drude weight and thermal Meissner stiffness coincide. We can thus compare the result from the Bethe ansatz with the CFT prediction. Recalling (39), the ground state energy in the presence of boost at low temperature is

$$E = E_\infty - \frac{c\pi v_s}{6L}\frac{1}{1 + v_s^2\kappa^2}. \tag{52}$$

Here, $c = 1$ is the central charge and $v_s = \frac{\pi\sin\gamma}{\gamma}$ is the sound velocity. With the identification $i\lambda = \kappa$, we obtain the CFT prediction

$$\bar{D}^Q = \frac{1}{2L}\frac{d^2E}{d\lambda^2}\Big|_{\lambda=0} = \bar{D}^Q_\infty - \frac{c\pi v_s^3}{6L^2}. \tag{53}$$

This is basically the same as (40). As shown in Fig. 6, the result from the Bethe ansatz agrees well with the CFT prediction, and converges to zero in the $L \to \infty$ limit as predicted [27].

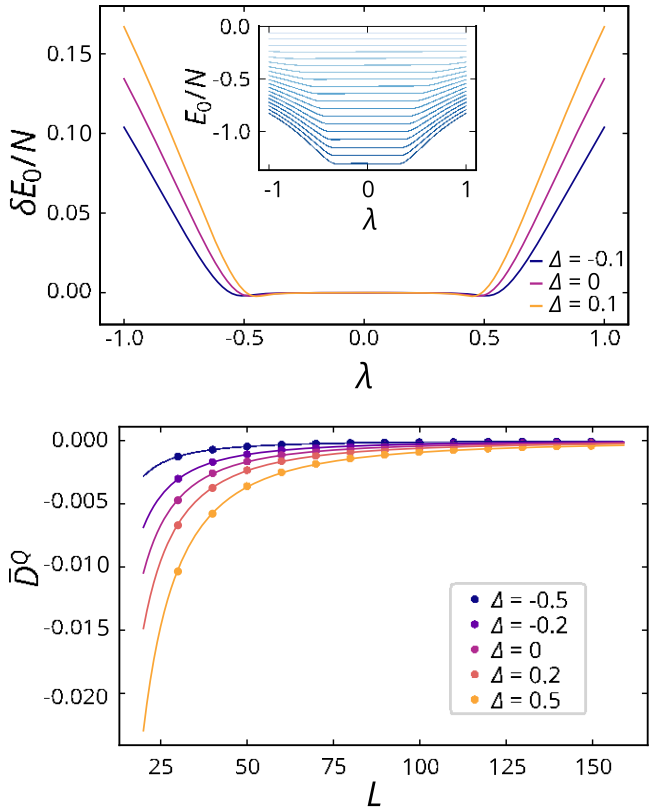

FIG. 6. (Top) The ground state energy of the boost-deformed XXZ model with $L = 100$ for $\Delta = -0.1, 0, 0.1$ computed from the boost-deformed Bethe ansatz equations. Here $\delta E_0 = E_0(\lambda) - E_0(0)$. The inset shows the ground state energy of the boost deformed XXZ model for $-0.9 \leq \Delta \leq 0.9$ with step size of 0.1 from top to bottom. (Bottom) The size dependence of the thermal Drude weight (26) at zero temperature calculated using the Bethe ansatz equations (dots). Solid lines represent the CFT predictions (40).

Using our formalism, it is also possible to discuss the nonlinear thermal Drude weights. They can be defined, following the definition of the nonlinear spin Drude weights [37,38], as

$$\bar{D}^{Q(n)} = \frac{1}{L}\frac{d^{n+1}E}{d\lambda^{n+1}}\bigg|_{\lambda=0}, \quad n > 1. \tag{54}$$

The results are shown in Fig. 7. From Fig. 7, we see that the CFT prediction still fits well the higher order nonlinear thermal Drude weight obtained from the Bethe ansatz, if we assume $\bar{D}_\infty^{Q(n=3,5)} = 0$: the nonlinear thermal Drude weights also converge to zero at large system sizes.

Finally, we can also obtain the nonlinear thermal Drude weights at finite boost parameter λ, as shown in Fig. 8. The nonlinear thermal Drude weights at zero temperature could be computed as

$$\bar{D}^{Q(n)}(\lambda) = \frac{1}{L}\frac{d^{n+1}E}{d\lambda^{n+1}} \propto \frac{1}{1 - v_s^2\lambda^2}. \tag{55}$$

Since $v_s = \frac{\pi \sin\gamma}{\gamma} \in (0, \pi)$, as we change Δ, there is a singularity at $v_s = 1/\lambda$. We indeed see in our Bethe ansatz calculation that at certain value of Δ, $D^{Q(n)}(\lambda)$ diverges for $\lambda = 0.5$ and $\lambda = 0.7$ (Fig. 8). We confirmed that these divergence values coincide with $v_s = 1/\lambda$.

These findings should be compared with the behaviors of the nonlinear spin Drude weights [37,39,40]. First, we did not observe divergences for $\bar{D}^{Q(n=3,5)}$ in contrast with the nonlinear spin Drude weights. Second, the Bethe ansatz results for $\bar{D}^{Q(n=3,5)}$ are described very well by the CFT predictions.

To address these questions (at least partially), let us focus on the noninteracting case and consider the effect of the nonlinearity of the dispersion on the nonlinear thermal Drude weight.[1] We consider the single particle spectrum:

$$\epsilon(p) = v_1 p + v_3 p^3 + \cdots = \sum_{m=1} v_{2m-1} p^{2m-1}. \tag{56}$$

As in Eq. (30), we impose the energy-twisted boundary condition,

$$p - \lambda \sum_{m=1} v_{2m-1} p^{2m-1} = \frac{2\pi}{L}(-r + \alpha), \quad r \in \mathbb{Z} \tag{57}$$

where $\alpha = 0(1/2)$ for PBC (APBC). This quantization condition on p can be solved order-by-order in λ. If we expand the momentum p as $p = \sum_{l=0} \lambda^l A_l$, we can determine A_l as

$$\begin{aligned} A_0 &= \frac{2\pi}{L}(-r + \alpha), \\ A_1 &= \sum_{m=1} v_{2m-1} A_0^{2m-1}, \\ A_2 &= \sum_{m=1} v_{2m-1}(2m-1) A_0^{2m-2} A_1, \\ &\vdots \\ A_l &= \sum_{m=1} v_{2m-1} \sum_{\substack{i_1 \le i_2 \le \cdots \le i_{2m-1} \\ i_1 r_1 + i_2 r_2 + \cdots = l-1}} C_{r_1, r_2 \cdots} A_{i_1}^{r_1} A_{i_2}^{r_2} A_{i_3}^{r_3} \cdots, \\ &\vdots \end{aligned} \tag{58}$$

with $C_{r_1, r_2, \ldots} = \frac{(2m-1)!}{r_1! r_2! \cdots}$. We assume the ground state where all single-particle states with $-r + \alpha < 0$ are filled. The ground state energy is then given by $E(\lambda) = \sum_{r=1}^{\infty} \sum_{m=1} v_{2m-1} p^{2m-1}(\lambda) = \sum_{r=1}^{\infty} \sum_{m=1} v_{2m-1} (\sum_{l=0} \lambda^l A_l)^{2m-1}$. The nonlinear thermal Drude weight is obtained by taking the (higher) derivative of the ground state energy with respect to λ. Focusing on the contributions from the linear part of the dispersion,

$$\frac{d^n E}{d\lambda^n} = \frac{n! v_1^{n+1} 2\pi}{L} \sum_{r=1}^{\infty} (-r + \alpha) + \cdots \tag{59}$$

We have so far focused on the left-movers. Combining the contributions from the right-movers, for which the dispersion is given by $\sum_m v_{2m-1}(-p)^{2m-1}$, we see that the contributions cancel for odd n, while they add up for even n. For APBC, we can regularize $\sum_{r=1}^{\infty}(-r + \alpha) = -1/24$. Hence,

$$\frac{d^n E}{d\lambda^n} = \begin{cases} -\dfrac{n! v_1^{n+1} \pi}{6L} & n : \text{even} \\ 0 & n : \text{odd} \end{cases}. \tag{60}$$

[1] We thank Hosho Katsura who suggested this calculation.

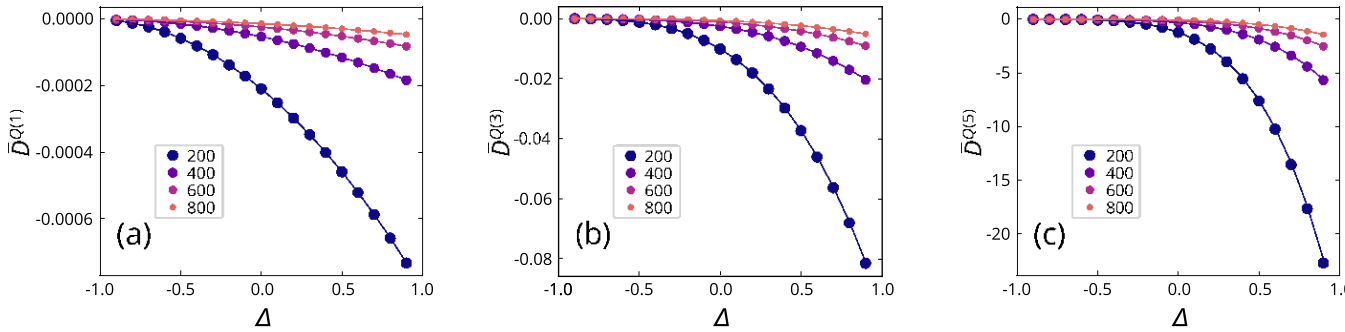

FIG. 7. The linear (a), third- (b), and fifth- (c) order nonlinear thermal Drude weights at $\lambda = 0$ as defined in Eq. (54) for different system sizes. The dots are from solving the Bethe ansatz and the solid lines are calculated from Eq. (54).

This is consistent with the calculation from Eq. (39) which suggests

$$E(\lambda) = -\frac{(c - 24h)\pi v}{6L(1 - v^2\lambda^2)} \tag{61}$$

(we take $c = 1$ and $h = 0$). The nonlinear thermal Drude weight is then

$$\bar{D}^{Q(n)} = \frac{1}{L}\frac{d^{(n+1)}E}{d\lambda^{(n+1)}} = \begin{cases} -\dfrac{(n+1)!v_1^{n+2}\pi}{6L^2} & n : \text{odd} \\ 0 & n : \text{even} \end{cases}. \tag{62}$$

To conclude, we see that the leading contributions to the nonlinear thermal Drude weights come from the linear part of the dispersion v_1. This should be contrasted with the nonlinear spin Drude weights, which are governed by the nonlinearity of the dispersion, $v_{2m-1>1}$ [41]. That is, the purely linearly-dispersing band or CFT predicts vanishing nonlinear spin Drude weights and fails to reproduce lattice calculations. On the other hand, for the nonlinear thermal Drude weight, CFT still captures the dominant contributions.

V. CONCLUSION

We have formulated a symmetry twist of the boundary condition relevant to thermal transport as the energy-twisted boundary condition, and shown that the stiffness against the twist quantifies thermal transport properties. We have also identified its bulk counterpart as the boost deformation, which has been studied in the context of a long-range deformation of integrable systems. These have a close analogy with the U(1) twisted boundary condition and the equivalent bulk U(1) gauge transformation relevant to electric transport. The relations have been confirmed by the agreement of the thermal Drude weight and the thermal Meissner stiffness estimated by each method. Specifically, the CFT result under the energy-twisted boundary condition agrees with the other results as far as CFT is applicable. A rigorous relation between the stiffnesses and the ac conductivity is shown only at the free fermion point.

The energy-twisted boundary condition is imposed on tori and is mostly suited for the evaluation of the partition function via the reconnection of tensor networks. It is thus compatible in particular with exact methods in 1 + 1 dimensions and numerical analysis in any dimensions. We have demonstrated how this method works in the estimation of the thermal Meissner stiffness of CFTs based on the modular transformation, and also that of the transverse-field Ising model and disordered lattice fermions in 1 + 1 dimensions based on the transfer matrix.

The boost deformation is a sort of integrable deformation applied in the bulk, and thus suited for integrable systems in 1 + 1 dimensions. We showed an implementation of the boost deformation in the Bethe ansatz, and addressed the linear and nonlinear thermal Drude weights of the XXZ Heisenberg spin chain. We also analyzed the energy-twisted deformation of the free fermion chain via the inviscid Burgers equation. The agreement of the thermal Meissner stiffness with that of the Ising CFT under the energy-twisted boundary condition

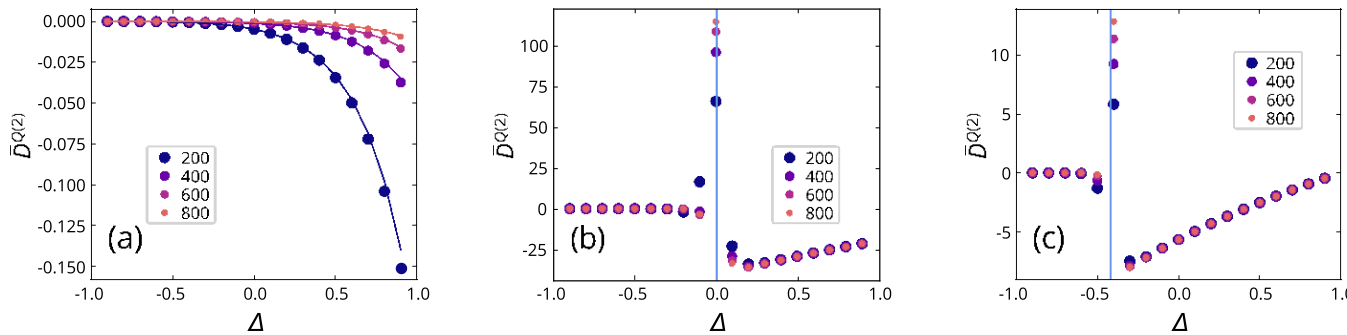

FIG. 8. The second-order nonlinear thermal Drude weight at $\lambda = 0.2$ (a), 0.5 (b), and 0.7 (c) for different system sizes. The dots are from solving the Bethe ansatz and the solid lines are calculated from Eq. (55). The blue vertical lines in (b) and (c) indicate the divergence region calculated from Eq. (55).

indicates an equivalence of the bulk and boundary-condition methods at least in a critical model.

Extending these analyses to a wider range of systems, beyond those studied in this paper, is an important open question. In particular, unlike the energy-twisted boundary condition, the boost deformation is formulated by making use of the integrability of (1+1)D quantum many-body systems, or in continuum systems with Lorentz invariance. It is important to formulate and study the boost deformation outside of these contexts. Also interesting is to study the energy-twisted boundary condition and boost deformation in quantum many-body systems in higher dimensions. As a simple warm-up, in Appendix E, we present the implementation of the energy-twisted boundary condition in the 2d integer quantum Hall effect. Just like Laughlin's argument for the quantized Hall conductance, the transverse energy transport can be induced by an adiabatic change in the boost parameter. Studying interacting 2d quantum many-body systems (e.g., fractional quantum Hall systems) using the energy-twisted boundary condition and boost deformation would be a natural next step. In this regard, it would be interesting to make a comparison with other formalisms, such as Ref. [42].

ACKNOWLEDGMENTS

We thank Vir Bulchandani, Hosho Katsura, Jonah Kudler-Flam, Kentaro Nomura, and Kiyohide Nomura for discussions. R.N. is supported by JSPS KAKENHI Grant No. JP17K17604 and JST CREST Grant No. JPMJCR18T2. S.R. is supported by the National Science Foundation under Award No. DMR-2001181, and by a Simons Investigator Grant from the Simons Foundation (Award No. 566116). This work is supported by the Gordon and Betty Moore Foundation through Grant No. GBMF8685 toward the Princeton theory program. This work was performed in part at Aspen Center for Physics, which is supported by National Science Foundation Grant No. PHY-1607611. This work was partially supported by a grant from the Simons Foundation.

APPENDIX A: GRAVIPHOTON FIELD ON 2-TORUS

Consider the (1+1)D Euclidean space-time with the metric

$$ds^2 = \left(d\tau + A_x^{\mathrm{E}} dx\right)^2 + dx^2, \tag{A1}$$

where A_x^{E} is the background gravitomagnetic vector potential. By the Wick rotation, $\tau = it$ and $A_x^{\mathrm{E}} = iA_x^{\mathrm{g}}$, the line element in the Minkowski signature is given by $ds^2 = -(dt + A_x^{\mathrm{g}} dx)^2 + dx^2$. The gravitomagnetic vector potential induces a gravitational counterpart of magnetic flux. Provided that the gravitomagnetic vector potential A_x^{E} is static, the metric (A1) is obtained from the regular flat metric by a transformation

$$(\tau, x) \to (\tau + \beta a(x), x), \tag{A2}$$

where $a(x) = \beta^{-1} \int_0^x dx^0 A_x^{\mathrm{E}}(x^0)$. To be consistent with the spatial periodicity, we assume A_x^{E} is a periodic function of x, $A_x^{\mathrm{E}}(x + L) = A_x^{\mathrm{E}}(x)$. If we start from the space-time 2-torus with periodicity

$$(\tau, x) \sim (\tau + \beta, x) \sim (\tau, x + L), \tag{A3}$$

then after the transformation the new identification condition is given by [6]

$$(\tau, x) \sim (\tau + \beta, x) \sim (\tau + \beta a(L), x + L). \tag{A4}$$

APPENDIX B: LATTICE SPIN SYSTEMS AND TRANSFER MATRIX FORMALISM

In this Appendix, we review the derivation of the column-to-column transfer matrix of the transverse-field Ising model following [43–47] and derive the twisted partition function. Consider the transverse-field Ising model in a general form

$$H = \sum_{i=1}^{L} \left(- J_i \sigma_i^x \sigma_{i+1}^x - h_i \sigma_i^z \right), \tag{B1}$$

satisfying PBC ($\sigma_{L+1} = \sigma_1$). By Trotterizing the imaginary time direction, the partition function is written in terms of the row-to-row transfer matrix V as $Z = \mathrm{Tr}\, e^{-\beta H} = \mathrm{Tr}\, V^M$, where an integer M is the length of the temporal direction. The transfer matrix can be written as a product form, $V = V^{(1)1/2} V^{(2)} V^{(1)1/2}$, where

$$V^{(1)} = \prod_{i=1}^{L} e^{\gamma_i \sigma_i^z}, \qquad V^{(2)} = \prod_{i=1}^{L} e^{K_i \sigma_i^x \sigma_{i+1}^x}. \tag{B2}$$

Here, the coefficients are defined by $K_i = \beta J_i / M$ and $\gamma_i = \beta h_i / M$. By introducing vectors $B_0(\lambda) = (\sqrt{\cosh \lambda}, 0)^T$ and $B_1(\lambda) = (0, \sqrt{\sinh \lambda})^T$, we obtain [46]

$$e^{K_i \sigma_i^x \sigma_{i+1}^x} = \sum_{s_i, t_{i+1}} B_{s_i}^T(K_i) B_{t_{i+1}}(K_i) \left| \sigma_i^x \right|_{s_i} \left| \sigma_{i+1}^x \right|_{t_{i+1}}, \tag{B3}$$

where s_i and t_{i+1} take 0,1, and thus

$$V^{(2)} = \sum_{s_1, t_1, k_2, \cdots, k_L} B_{s_1}^T(K_1) C_2^{k_2} \cdots C_L^{k_L} B_{t_1}(K_L) \times \left| \sigma_1^x \right|_{s_1 + t_1} \otimes \left| \sigma_2^x \right|_{k_2} \otimes \cdots \otimes \left| \sigma_L^x \right|_{k_L}, \tag{B4}$$

where $C_i^k = \sum_s B_s(K_{i-1}) B_{s+k}^T(K_i)$ and the subscript of $B_s(\lambda)$ is defined modulo 2. By making the imaginary-time coordinate explicit, we obtain $V^M = \bigotimes_{j=1}^{M} V_j$ where

$$V_j = \sum_{s_{1j}, t_{1j}, k_{2j}, \cdots, k_{Lj}} B_{s_{1j}}^T(K_1) C_{2j}^{k_{2j}} \cdots C_{Lj}^{k_{Lj}} B_{t_{1j}}(K_L) \times X_{1j}^{s_{1j} + t_{1j}} \otimes X_{2j}^{k_{2j}} \otimes \cdots \otimes X_{Lj}^{k_{Lj}} \tag{B5}$$

and $X_{ij}^k = e^{\gamma_i \sigma_i^z / 2} (\sigma_i^x)^k e^{\gamma_i \sigma_i^z / 2}$.

When the space-time is twisted by a lattice sites, Ising coupling connects the boundary spin at a position (L, j) to the spin on the other side at $(1, j + a)$. This changes the ket vector in (B5) as $B_{t_{1j}}(K_L) \to B_{t_{1\,j+a}}(K_L)$. Inserting the identity matrix $\mathbf{1} = \sum_{\tau_j} |\tau_j\rangle\langle\tau_j|$ of the auxiliary two-dimensional space in front of $B_{t_{1\,j+a}}(K_L)$, the transfer matrix on a twisted space-time becomes

$$V_j(a) = \sum_{\tau_j} \sum_{k_{1j}, \cdots, k_{Lj}} \langle \tau_{j-a} | C_{1j}^{k_{1j}} \cdots C_{Lj}^{k_{Lj}} | \tau_j \rangle \times X_{1j}^{k_{1j}} \otimes X_{2j}^{k_{2j}} \otimes \cdots \otimes X_{Lj}^{k_{Lj}} \tag{B6}$$

Due to the duality between C and X, the column-to-column transfer matrix is

$$W_i = \sum_{\sigma_i} \sum_{k_{i1},\cdots,k_{iM}} \langle\sigma_i|X_{i1}^{k_{i1}}\cdots X_{i1}^{k_{iM}}|\sigma_i\rangle \times C_{i1}^{k_{i1}} C_{i2}^{k_{i2}} \cdots C^{k_{iM}}_{iM} \tag{B7}$$

which satisfies $Z = \sum_{\sigma} \langle\sigma_1\cdots\sigma_L|\prod_j V_j(a)|\sigma_1\cdots\sigma_L\rangle = \sum_{\tau} \langle\tau_{1-a}\cdots\tau_{M-a}|\prod_i W_i|\tau_1\cdots\tau_M\rangle$. Here, the auxiliary spin is also periodically identified: $\tau_{j+M} = \tau_j$.

The spin operators C and X can be rewritten by a similar expression as the original X and C, respectively, as

$$C_{ij}^k = \alpha_i e^{K_{i-1}\tau_j^z/2} \tau_j^x e^{K_i^k \tau_j^z/2}, \tag{B8}$$

$$X_{ij}^k = \beta_i \sum_s B_s(\gamma_i^k) B_{s+k}^T(\gamma_i^k), \tag{B9}$$

where $\tanh K_i = e^{-2K_i^k}$ and $\tanh\gamma_i = e^{-2\gamma_i^k}$ from the standard notation [34], $\alpha_i = (\sinh 2K_{i-1}\sinh 2K_i/4)^{1/4}$, and $\beta_i = (2\sinh 2\gamma_i)^{1/2}$. Notice that the vector $B_s(^2)$ in (B9) is the spinor of the real spin σ, while that in (B3) is of the auxiliary spin τ. These expressions lead to the column-to-column transfer matrix in terms of the auxiliary spin as $W_i = (\alpha_i\beta_i)^M W_{i-1}^{(1)1/2} W_i^{(2)} W_i^{(1)1/2}$, where

$$W_i^{(1)} = \prod_{j=1}^M e^{K_i^k \tau_j^z}, \quad W_i^{(2)} = \prod_{j=1}^M e^{\gamma_i^k \tau_j^x \tau_{j+1}^x}. \tag{B10}$$

The transfer matrix is diagonalized by introducing fermionic representation via the Jordan-Wigner transformation: $\tau_j^z = 2c_j^\dagger c_j - 1$, $\tau_j^+ = \tau_j^x + i\tau_j^y = 2e^{i\pi\sum_{l<j} c_l^\dagger c_l} c_j^\dagger$. The Ising coupling is then written by the hopping of the Jordan-Wigner fermions as

$$\tau_j^x \tau_{j+1}^x = (c_j^\dagger - c_j)(c_{j+1}^\dagger + c_{j+1}), \tag{B11}$$

where, at the boundary, $c_{M+1} = -e^{i\pi\sum_j c_j^\dagger c_j} c_1$ is imposed. Since the Hamiltonian is bilinear in the fermion operators, the total fermion number $F = \sum_j c_j^\dagger c_j$ modulo 2 is conserved. The Fock space is then decomposed into even- and odd-fermion-number subspaces, within which the fermion operator obeys APBC and PBC, respectively. The boundary condition in the temporal direction appears in the frequencies of the Fourier mode:

$$c_j = \frac{e^{-i\pi/4}}{\sqrt{M}} \sum_\omega e^{i\omega j} c_\omega, \tag{B12}$$

where

$$\omega = \begin{cases} \pm\frac{\pi}{M}, \pm\frac{3\pi}{M}, \cdots, \pm\frac{(M-1)\pi}{M} & (F:\text{even}) \\ 0, \pm\frac{2\pi}{M}, \cdots, \pm\frac{(M-2)\pi}{M}, \pi & (F:\text{odd}) \end{cases} \tag{B13}$$

for even M and

$$\omega = \begin{cases} \pm\frac{\pi}{M}, \pm\frac{3\pi}{M}, \cdots, \pm\frac{(M-2)\pi}{M}, \pi & (F:\text{even}) \\ 0, \pm\frac{2\pi}{M}, \cdots, \pm\frac{(M-1)\pi}{M} & (F:\text{odd}) \end{cases} \tag{B14}$$

for odd M. The transfer matrix is then written as

$$W_i = \prod_{\omega\in[0,\pi]}{}' W_i(\omega), \tag{B15}$$

where the summation is over the non-negative part of (B13) and (B14), and by using $n_\omega = c_\omega^\dagger c_\omega$,

$$W_i(0) = e^{(K_{i-1}+2\gamma_i+K_i)(n_0-1/2)}, \tag{B16}$$

$$W_i(\pi) = e^{(K_{i-1}-2\gamma_i+K_i)(n_\pi-1/2)}, \tag{B17}$$

$$W_i(\omega) = e^{K_{i-1}(n_\omega+n_{-\omega}-1)} \times e^{2\gamma_i(\cos\omega(n_\omega+n_{-\omega})+\sin\omega(c_{-\omega}^\dagger c_\omega^\dagger + c_\omega c_{-\omega}))} \times e^{K_i(n_\omega+n_{-\omega}-1)}, \tag{B18}$$

We can decompose the Fock space into subspaces specified by Fourier components of $\omega = 0, \pi$, and combined ω and $-\omega$. To be specific, the $\omega = 0/\pi$ subspace is spanned by $|0\rangle$ and $c_{0/\pi}^\dagger|0\rangle$, and a $\omega = 0,\pi$ subspace by $|0\rangle$, $c_\omega^\dagger|0\rangle$, $c_{-\omega}^\dagger|0\rangle$, and $c_{-\omega}^\dagger c_\omega^\dagger|0\rangle$. The trace of the column-to-column transfer matrix (B15) is thus the product of the traces of small matrices corresponding to the subspaces.

When the space-time is twisted, the fermion operators at $i = 1$ are changed as $c_m \to c_{m+a}$, which shifts the Fourier mode by a frequency-dependent phase as

$$c_\omega \to e^{ia\omega} c_\omega. \tag{B19}$$

This modifies the trace operation so that the bra vector is shifted by a phase determined by the number of fermion and the frequency as

$$\langle n_0| \to \langle n_0|, \quad \langle n_\pi| \to (-1)^{an_\pi}\langle n_\pi|, \quad \langle n_\omega n_{-\omega}| \to e^{ia\omega(n_\omega-n_{-\omega})}\langle n_\omega n_{-\omega}|. \tag{B20}$$

Finally, the partition function after the twist is the sum of contributions from even- and odd-fermion-number spaces as

$$Z(a) = \sum_{\pm} \prod_{\omega\in[0,\pi]}{}' \mathrm{Tr}_\omega^\pm \frac{1+(-1)^F}{2} \prod_{i=1}^L W_i(\omega), \tag{B21}$$

where the first summation is over the even- and odd-fermion-number spaces, and Tr_ω^0 is the trace over a ω subspace with the modified bra vector (B20). A proportionality constant $(\alpha_i\beta_i)^{LM}$ is omitted. Specifically, the trace of a twisted $\omega = 0$ subspace is

$$\mathrm{Tr}_\omega^0 (\pm 1)^F \prod_{i=1}^L W_i(\omega) = \begin{pmatrix} \langle 0| \\ \pm e^{ia\omega}\langle 0|c_\omega \\ \pm e^{-ia\omega}\langle 0|c_{-\omega} \\ \langle 0|c_\omega c_{-\omega} \end{pmatrix}^T \prod_{i=1}^L W_i(\omega) \begin{pmatrix} |0\rangle \\ c_\omega^\dagger|0\rangle \\ c_{-\omega}^\dagger|0\rangle \\ c_{-\omega}^\dagger c_\omega^\dagger|0\rangle \end{pmatrix} \tag{B22}$$

The matrix element of the Fourier-decomposed transfer matrix $W_i(\omega)$ can be found in [34].

APPENDIX C: TRANSFER MATRIX METHOD FOR FREE FERMION MODELS

Following [48], we consider the free fermion model on a 1d lattice with the Hamiltonian

$$H = \sum_i h_{i,i+1} = -\sum_i t_i (c_i^\dagger c_{i+1} + \text{H.c.}) + \sum_i (U_i - \mu) c_i^\dagger c_i. \tag{C1}$$

To implement the transfer matrix method, we decompose the system into even and odd sites and define $H_1 = \sum_{i=\text{odd}} h_{i,i+1}$, $H_2 = \sum_{i=\text{even}} h_{i,i+1}$. With the local transfer matrices defined as $V_1 = e^{-\tau H_1} = \prod_{i=\text{odd}} v_{i,i+1}$, and $V_2 = e^{-\tau H_2} = \prod_{i=\text{even}} v_{i,i+1}$, where $v_{i,i+1} = e^{-\tau h_{i,i+1}}$, the partition function can be written as

$$Z = \text{Tr}\,(e^{-\beta H}) = \text{Tr}\,(V_1 V_2)^M + O(\tau^2), \tag{C2}$$

where $\tau = \beta/M$ and M is Trotter number. By inserting the complete set of states, we can write the row-to-row partition function as

$$Z = \sum_{\{n_i^l\}} \prod_{l=1}^{M} \langle n^{2l-1,2l} | v^{1,2} \cdots v^{N-1,N} | n^{2l,2l+1} \rangle \langle n^{2l,2l+1} | v^{2,3} \cdots v^{N,1} | n^{2l-1,2l} \rangle, \tag{C3}$$

where $v^{l,l+1} = \langle n^l, n^{l+1} | v_{i,i+1} | n^{l+1}, n^{l+1} \rangle$ with i and l represent the site number in space and Trotter directions, respectively.

In order to go from the row-to-row to column-to-column transfer matrix, we rotate each block as

$$\tau_{i,i+1}^{l,l+1} = \langle n_i^l, 1 - n_i^{l+1} | v_{i,i+1} | 1 - n_{i+1}^l, n_{i+1}^{l+1} \rangle. \tag{C4}$$

Explicitly, it is given by

$$\tau_{i,i+1}^{l,l+1} = b_i \begin{bmatrix} u_i & 0 & 0 & 0 \\ 0 & a_i - w_i & b_i^{-1} & 0 \\ 0 & b_i & a_i + w_i & 0 \\ 0 & 0 & 0 & u_i \end{bmatrix} \tag{C5}$$

in the basis of $\{|00\rangle, |01\rangle, |10\rangle, |11\rangle\}$ with parameter defined as

$$\begin{aligned} \alpha_i &= \frac{-\tau(\epsilon_i - \mu)}{U2}, \quad \gamma_i = \sqrt{\alpha_i^2 + \tau^2 t_i^2}, \\ b_i &= e^{\alpha_i}, \quad u_i = \frac{\tau t_i \sinh \gamma_i}{\gamma_i}, \\ a_i &= \cosh \gamma_i, \quad w_i = \frac{\alpha_i \sinh \gamma_i}{\gamma_i}. \end{aligned} \tag{C6}$$

Therefore the partition function in terms of the column-to-column transfer matrices is written as

$$Z = \text{Tr}\,[T_{1,2} T_{2,3} \cdots T_{N,1}], \quad T_{i,i+1} = \prod_l \tau_{i,i+1}^{l,l+1}. \tag{C7}$$

Once we write the partition in the matrix form, we can perform the Fourier transform in the Trotter direction, and the partition function can be written as

$$Z = \prod_i C_i^M \prod_\omega \text{Tr}\,[2 + T_\omega], \quad T_\omega = \prod_{i=1}^{N/2} t_{2i-1} t_{2i,\omega}, \tag{C8}$$

where $C_i = u_i b_i$, and t_{2i-1} and $t_{2i,\omega}$ are defined as

$$t_{2i-1} = \frac{1}{u_{2i-1}} \begin{bmatrix} a_{2i-1} - w_{2i-1} & b_{2i-1}^{-1} \\ b_{2i-1} & a_{2i-1} + w_{2i-1} \end{bmatrix}, \tag{C9}$$

$$t_{2i} = \frac{1}{u_{2i}} \begin{bmatrix} a_{2i} + w_{2i} & e^{-i\omega} b_{2i} \\ e^{i\omega} b_{2i}^{-1} & a_{2i} - w_{2i} \end{bmatrix}. \tag{C10}$$

We use the even number of Trotter sites, and hence $\omega = \frac{(2m+1)\pi}{M}$ with $m = -\frac{M}{2}, \cdots -1, 0, \cdots \frac{M}{2} - 1$.

1. Phase-twisted boundary condition

Now we consider the system with phase twisted boundary condition, i.e., $t_N \to t_N e^{2\pi i\varphi}$ where $\varphi = \theta/\theta_0$. This results in the change of the parameter u_N in the transfer matrix $\tau_{N,1}$,

$$\tau_{N,1}^{l,l+1} = b_N \begin{bmatrix} u_N & 0 & 0 & 0 \\ 0 & a_N - w_N & b_N^{-1} & 0 \\ 0 & b_N & a_N + w_i & 0 \\ 0 & 0 & 0 & u_N \end{bmatrix}. \tag{C11}$$

Accordingly, the modified partition function is

$$Z = \prod_i C_i^M \prod_\omega \text{Tr}\,[2\cos(2\pi\varphi) + T_\omega]. \tag{C12}$$

We use $M = 2N$ to ensure the convergence of the partition function. The results are shown in Fig. 9. The period of φ is 1 which is equal to a phase twist of 2π. Here we consider the system with on-site random potential U_i to be Gaus-sian distributed with variance σ. We see that as the disorder strength increases, the free energy curves become more flat which means the system is more localized and less sensitive to boundary conditions.

Then we compute the electrical Meissner stiffness $D = (2L)^{-1} d^2F/d\varphi^2$ (Fig. 9). For the clean free fermion system (black), we observe the electrical Meissner stiffness decays algebraically as $D \propto L^{-2}$ for $L \gg \beta$, which we confirmed is consistent with the analytical result. (Here, we take the parameter $\beta = 500$.) On the other hand, for the high temperature (long wire) regime, $\beta \gg L$, the Meissner stiffness decays exponentially.

We also studied two types of disordered fermion chains, one with on-site disorder, and the other with bond disorder. Here, for the on-site randomness, we consider U_i to be Gaus-sian distributed with variance σ. For the random hopping model, the hopping amplitudes are drawn from a uniform distribution, $t_{i,i+1} \in [1 - \sigma, 1 + \sigma]$. We focus on the length regime $\ell \gg L \gg \beta$, where ℓ is the mean free path.

For the case of on-site disorder, we see that as the disorder strength increases (σ increases), the Meissner stiffness decreases as expected. The algebraically decaying part follows L^{-2} and the exponents of the exponentially decaying part grows as disorder strength is increased. Such behavior fits the Anderson localization picture where the localization length decreases as the disorder strength increases. A similar behavior is also observed for the random hopping model, where the electrical Meissner stiffness also follows algebraically and exponentially decay. We note that the electrical conductance for the random hopping model is known to decay algebraically, $g \propto 1/\sqrt{L}$. The exponentially decaying part could be explained by the normalization of energy level spacing.

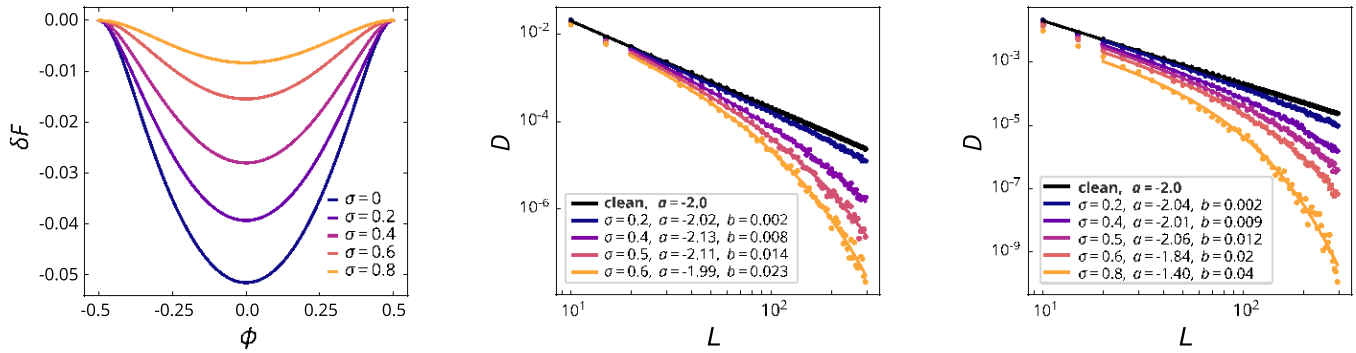

FIG. 9. (Left) The U(1)-phase-twist variation of the free energy of the free fermion model with random on-site potential. The curves are shown as varying σ from 0 to 0.8. The calculation is done with $L = 50$ and $\beta = 100$. The electrical Meissner stiffness for the disordered free fermion chain with random on-site potential (middle) and with random hopping (right). Dots represents the results from the transfer matrix method and solid lines are fitting with $D \propto L^{a} e^{-L/b}$. The fitting parameter are labeled in plots with $\beta = 500$.

2. Energy-twisted boundary condition

We now turn to the energy-twisted boundary condition. It can be implemented in the column-to-column transfer matrix method as

$$Z = \mathrm{Tr}\,[T_{1,2} \cdots T_{N-1,N} e^{iP1\tau}]. \tag{C13}$$

Similar to the phase-twisted boundary condition, the energy twist results in the coupling $t_{i,i+1} \to t_{i,i+1} e^{i\omega M\kappa}$ where ω is the frequency in the Trotter direction. Therefore, following the same calculation as the phase twist, the partition function can be written as

$$Z = \prod_i C_i^M \prod_\omega \mathrm{Tr}\,[2\cos(\omega M\kappa) + T_\omega]. \tag{C14}$$

The energy-twisted free energy and the thermal Meissner stiffness, computed by the transfer matrix method, are plotted in Fig. 10. As before, we study the clean fermion model, the disordered model with on-site disorder, and the random hopping model. For the free energy plot, we consider the system with on-site random potential U_i to be Gaussian distributed with variance σ. We could see that as the disorder strength increases, the free energy curves become more flat, which means the system is more localized and less sensitive to boundary conditions.

For the clean system, we checked that the thermal Meissner stiffness decays algebraically as $D^Q \propto L^{-4}$ (for $L \gg \beta$), which agrees with the CFT prediction $d^2F/d\kappa^2 \propto L^{-3}$. For the case of on-site disorder, the algebraically decaying part generally follows $D^Q \propto L^{-4}$. As the disorder is stronger, the thermal Meissner stiffness decays exponentially with length as expected from Anderson localization. The exponent represents the inverse of the localization length and it increases as the disorder is stronger.

For the random hopping model, the thermal Meissner stiffness also shows algebraic and exponential decay as the case of Anderson localization. The electrical conductance of the random hopping model decays algebraically as $g \propto 1/\sqrt{L}$. Due to the Wiedemann-Franz law, we expect the thermal conductance also behaves similarly. The conductance is given by $g \propto E/\Delta$ with E being the sensitivity of the energy to the twisted boundary condition and $\Delta = 1/\rho(0)$ is the energy level spacing at zero energy. The exponential decay might be due to the zero energy level spacing of the random hopping model.

APPENDIX D: BOOST DEFORMATION AND THERMAL RESPONSE

In this section, we show that the thermal Drude weight and thermal Meissner stiffness of a disordered lattice fermion are

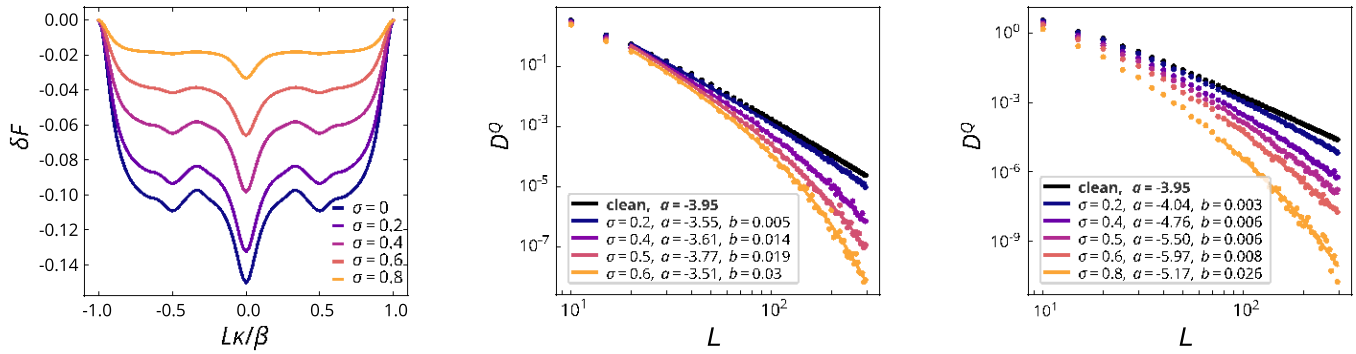

FIG. 10. (Left) The energy-twist variation of the free energy of the free fermion model with random on-site potential. The curves are shown as varying σ from 0 to 0.8. The calculation is done with $L = 20$ and $\beta = 100$. The thermal Meissner stiffness for the disordered free fermion chain with random on-site potential (middle), and with random hopping (right). Dots represent the results from the transfer matrix method with $\beta = 500$ and solid lines are fitting with $D_Q \propto L^{a} e^{-L/b}$.

related to the boost deformation via (26) and (27). The argument in this section is basically in parallel with the analogous U(1) twist.

1. Thermal conductivity

First, we review the thermal Drude weight $\bar{D}^Q$ and the thermal Meissner stiffness D^Q following [14].

The ac thermal conductivity of a local Hamiltonian $H_0 = \sum_i H_i$ coupled with a gravitational field $\psi_j(t) = e^{iqj-i(\omega+i\eta)t}$, serving as a temperature profile via $\nabla\psi(r) = -[\nabla T(r)]/T(r)$, is given in (25) in the limit of $q \to 0$, where

$$D^Q = \frac{1}{2L}\left(\langle 2\rangle - \int_0^\beta d\tau \langle J^Q(-i\tau)J^Q\rangle\right), \tag{D1}$$

$$\kappa_{\mathrm{KG}}(\omega) = -\frac{1}{LT}\int_{-\infty}^{0} dt\, e^{-i(\omega+i\eta)t}\int_0^\beta d\tau \langle J^Q(t-i\tau)J^Q\rangle. \tag{D2}$$

Here, $A(t) = e^{itH_0}Ae^{-itH_0}$, $\langle A\rangle = \mathrm{Tr}[e^{-\beta H_0}A]/Z$, $Z = \mathrm{Tr}[e^{-\beta H_0}]$ is the partition function, and the heat current and thermal operators are

$$J^Q = \sum_j J_j^Q = -\frac{i}{2}\sum_{jk}(j-k)[H_j, H_k], \tag{D3}$$

$$2 = -\frac{1}{2}\sum_{jak}(j-k)(j-a)[[H_j, H_a], H_k]. \tag{D4}$$

Notice that these operators are defined unambiguously when the distance of two sites $j-k$ is uniquely defined, that is, when the Hamiltonian is local (the distance $|j-k|$ up to which $[H_j, H_k] = 0$ is bounded) or unless subject to PBC.

In terms of the eigenenergy E_n and eigenstates $|n\rangle$ of the Hamiltonian H_0, the thermal Drude weight is

$$\begin{aligned}\bar{D}^Q &= D^Q + \frac{1}{2LT}\sum_{E_n=E_m}\frac{e^{-\beta E_n}}{Z}|\langle n|J^Q|m\rangle|^2 \\ &= \frac{1}{2L}\left(\langle 2\rangle - 2\sum_{\substack{n,m\\ E_n=E_m}}\frac{e^{-\beta E_n}}{Z}\frac{|\langle n|J^Q|m\rangle|^2}{E_m-E_n}\right).\end{aligned} \tag{D5}$$

In the limit of vanishing temperature ($T \to 0$) while keeping the system size finite ($L < \infty$), the thermal Drude weight and the thermal Meissner stiffness coincide unless the ground state is degenerate.

When a disordered, free lattice fermion Hamiltonian

$$H_0 = \sum_{jk}^{L} t_{jk}c_j^\dagger c_k \tag{D6}$$

is considered, the above operators are given, respectively, by

$$J^Q = -\frac{i}{2}\sum_{jak}^{L}(j-k)t_{ja}t_{ak}c_j^\dagger c_k, \tag{D7}$$

$$2 = -\frac{1}{4}\sum_{jabk}^{L}(j-k)(j+a-b-k)t_{ja}t_{ab}t_{bk}c_j^\dagger c_k. \tag{D8}$$

2. Boost deformation

We consider a disordered lattice fermion model and the corresponding boost operator given by

$$H(\lambda) = \sum_{jk} t_{jk}(\lambda)c_j^\dagger c_k, \tag{D9}$$

$$B[H(\lambda)] = \sum_{jk}\frac{j+k}{2}t_{jk}(\lambda)c_j^\dagger c_k. \tag{D10}$$

The boost deformation (12) is reduced to

$$\frac{dt_{jk}(\lambda)}{d\lambda} = \frac{i(j-k)}{2}\sum_a t_{ja}(\lambda)t_{ak}(\lambda), \tag{D11}$$

and from this equation the second derivative is

$$\frac{d^2t_{jk}(\lambda)}{d\lambda^2} = -\frac{j-k}{4}\sum_{ab}(j+a-b-k)t_{ja}(\lambda)t_{ab}(\lambda)t_{bk}(\lambda). \tag{D12}$$

Notice that we adopted a specific Hamiltonian (D9) since the second derivative of a general local Hamiltonian $H = \sum H_j$ cannot be obtained in this way. Referring to (D7) and (D8), the deformed Hamiltonian is expanded around $\lambda = 0$ as

$$H(\lambda) = H(\lambda=0) - \lambda J^Q + \frac{\lambda^2}{2}2 + O(\lambda^3), \tag{D13}$$

where the operators J^Q and 2 are defined with hopping parameters before the deformation $t_{jk}(\lambda = 0)$.

From (D13), the perturbative expansion of an eigenenergy up to the second order in the boost parameter is

$$\begin{aligned}E_n(\lambda) = E_n(\lambda=0) &- \lambda\langle n|J^Q|n\rangle \\ &+ \frac{\lambda^2}{2}\left(\langle n|2|n\rangle - 2\sum_{\substack{m\\ E_n(0)=E_m(0)}}\frac{E|\langle n|J^Q|m\rangle|^2}{E_n(0)-E_m(0)}\right),\end{aligned} \tag{D14}$$

which gives a relation between the thermal Drude weight (D5) and the boost deformation as shown in (26).

On the other hand, the derivative of the free energy $F(\lambda) = -\beta^{-1}\ln Z(\lambda)$ is, by using (D13) and the absence of the heat current $\langle J^Q\rangle = -dF/d\lambda|_{\lambda=0}$ in the ground state,

$$\frac{d^2F(\lambda)}{d\lambda^2}\Big|_{\lambda=0} = \langle 2\rangle - \int_0^\beta d\tau\langle J^Q(-i\tau)J^Q\rangle, \tag{D15}$$

which leads to the relation (27) between the thermal Meissner stiffness and the derivative of the free energy.

3. A clean system in the thermodynamic limit

We rederive the thermal Drude weight and thermal Meissner stiffness of a clean lattice fermion in the thermodynamic limit [14] by using the boost deformation. When spatial translation symmetry is present and in the thermodynamic limit $L \to \infty$, the single-particle eigenenergy $\epsilon_q = \sum_j t_{j,j+a}e^{iqa}$ is a differentiable function of the momentum q_a and the

boost parameter λ, and thus the heat current and thermal operators are

$$J^Q = -\sum_q \frac{\partial \epsilon_q}{\partial \lambda} c_q^\dagger c_q = \sum_q \epsilon_q \frac{\partial \epsilon_q}{\partial q} c_q^\dagger c_q, \tag{D16}$$

$$2 = \sum_q \frac{\partial^2 \epsilon_q}{\partial \lambda^2} c_q^\dagger c_q = \sum_q \left(\frac{\partial}{\partial q} \epsilon_q \frac{\partial \epsilon_q}{\partial q} \right) c_q^\dagger c_q, \tag{D17}$$

where $c_q = L^{-1/2} \sum_j e^{iqj} c_j$. The derivatives of the averaged many-body eigenenergy E_n and the free energy $F = -\beta^{-1} \sum_q \ln(1 + e^{-\beta \epsilon_q})$ are

$$\sum_n \frac{e^{-\beta E_n}}{Z} \frac{d^2 E_n}{d\lambda^2} = \sum_q f(\epsilon_q) \frac{\partial^2 \epsilon_q}{\partial \lambda^2}, \tag{D18}$$

$$\frac{d^2 F}{d\lambda^2} = \sum_q \left[f'(\epsilon_q) \frac{\partial^2 \epsilon_q}{\partial \lambda^2} + \frac{df(\epsilon_q)}{d\epsilon_q} \left(\frac{\partial \epsilon_q}{\partial \lambda} \right)^2 \right], \tag{D19}$$

where f is the Fermi distribution function. Substituting into (26) and (27), we obtain

$$\bar{D}^Q = \frac{1}{4\pi} \int dq \left(-\frac{df}{d\epsilon_q} \right) \left(\epsilon_q \frac{\partial \epsilon_q}{\partial q} \right)^2 = \frac{\pi}{12\beta^2} \sum_{\mathrm{FP}} |v_F|, \tag{D20}$$

$$D^Q = \frac{1}{4\pi} \int dq \frac{\partial}{\partial q} \left[f(\epsilon_q) \epsilon_q^2 \frac{\partial \epsilon_q}{\partial q} \right] = 0, \tag{D21}$$

where FP stands for the Fermi points.

4. Finite-length behavior

In this section, we see that the thermal Meissner stiffness at $T = 0$ depends qualitatively on the length modulo 4, and that they are related to the low-energy excitations.

Figure 11 shows the detailed length dependence of the thermal Meissner stiffness at $T = 0$ for PBC and APBC. When the length is $L = 4n (n \in \mathbf{N})$, the thermal Meissner stiffness of PBC scales as $2\pi v^3/6L^2$ while that of APBC scales as $-\pi v^3/6L^2$. However, when the length is $L = 4n + 2$, these behaviors are inverted. When the length is an odd integer ($L = 4n + 1$ or $4n + 3$), the thermal Meissner stiffness scales as $-(1/4)\pi v^3/6L^2$.

As was shown in Sec. III A, the thermal Meissner stiffness (40) of CFT at sufficiently low temperature is proportional to the ground state energy $E_0 = -(2\pi v/L)(c - 24h)/12$. A one-dimensional Dirac fermion is equivalent to two real fermions corresponding to the Ising CFT, and hence the ground state energy of the Dirac fermion is equal to twice that of the Ising CFT ($c = 1/2$). Specifically, when a boundary condition $\psi(x + L) = e^{2\pi i\alpha} \psi(x)$ where $\alpha \in [0, 1)$ is imposed, the single-particle eigenenergy of a chiral Dirac fermion $H = -iv\partial_x$ is $2\pi rv/L$ ($r \in \mathbf{Z} + \alpha$), and hence

$$H = \frac{2\pi v}{L} \sum_r r c_r^\dagger c_r = \frac{2\pi v}{L} \sum_r r : c_r^\dagger c_r : + E_0, \tag{D22}$$

where : : is the normal ordering, and via the zeta-function regularization,

$$E_0 = \frac{2\pi v}{L} \sum_{n=1}^{\infty} (-n + \alpha) = -\frac{2\pi v}{L} \left[\frac{1}{24} - \frac{1}{2} \left(\frac{1}{2} - \alpha \right)^2 \right]. \tag{D23}$$

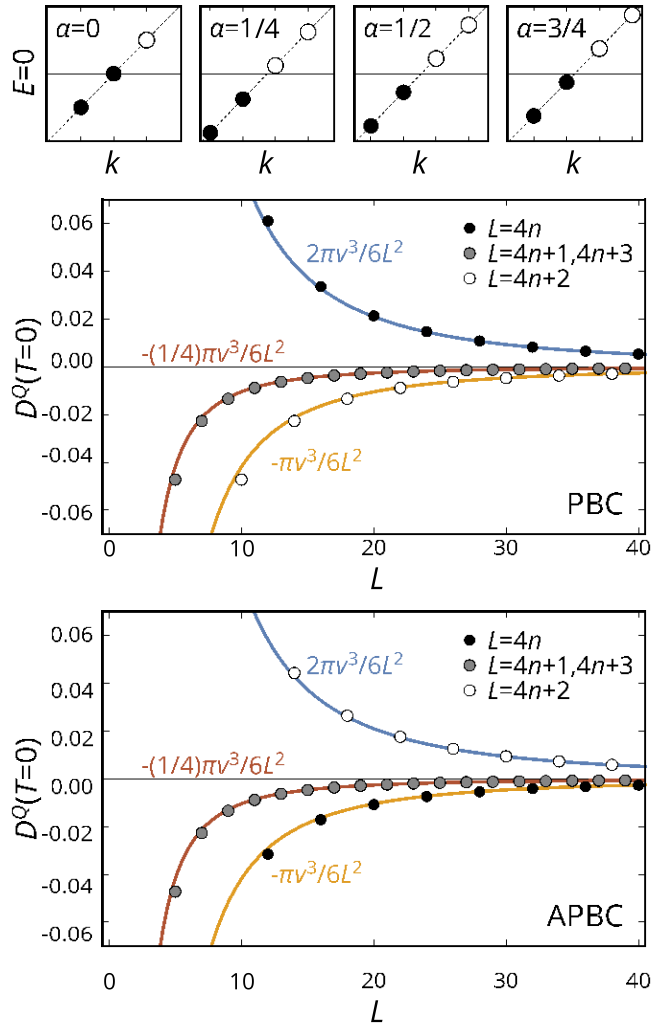

FIG. 11. Low energy excitations for $\alpha = 0, 1/4, 1/2$, and $3/4$. The thermal Meissner stiffness at zero temperature of a lattice free fermion is shown for PBC and APBC and is fitted by the corresponding CFT results.

As for the left mover, we impose $\psi(x + L) = e^{-2\pi i\alpha} \psi(x)$ to make α-dependence of the energy levels the same as the right one. Then the ground state energy of the helical Dirac fermion (including both left and right movers) with PBC ($\alpha = 0$) is $E_0 = (1/6)(2\pi v/L)$ that corresponds to twice the ground state energy of CFT with $c = 1/2$ and $h = 1/16$, and that with APBC ($\alpha = 1/2$) is $E_0 = (-1/12)(2\pi v/L)$ corresponding to $c = 1/2$ and $h = 0$.

To make a connection to the lattice fermion, we naively anticipate that the ground state energy used for deriving the thermal Meissner stiffness can be identified with that of the linearized helical Dirac fermion, since low-energy states are relevant to low-temperature behavior. In doing so, we notice that energy levels near the Fermi level depend on the length and the boundary condition (Fig. 11). Let us assume the cosine band $\epsilon_k = -2 \cos k$. With PBC and $L = 4n$, there are states $k_F = \pm\pi/2$ exactly at the Fermi level and thus the right and left movers correspond to $\alpha = 0$. Similarly, PBC with $L = 4n + 2$ corresponds to $\alpha = 1/2$, and PBC with $L = 4n + 1 (4n + 3)$ to $\alpha = 3/4 (1/4)$. Specifically, when the

length is odd, the ground state energy is $-(1/48)2\pi v/L$ from (D23), and the corresponding thermal Meissner stiffness is estimated as $D^{Q} = -(1/4)(\pi v^3/6L^2)$. Strictly speaking, the ground state energy obtained in this way is not the actual energy, but a quantity related to thermal response. When switched to APBC, the above results still hold by shifting $\alpha \to \alpha + 1/2$ mod 1, and hence this explains mod 4 behavior seen in Fig. 11. Notice that this argument is true when the chemical potential is 0, where α depends on the length only modulo 4.

APPENDIX E: QUANTUM HALL SYSTEMS WITH BOOST DEFORMATION

In this Appendix, we consider the boost deformation of the quantum Hall system. We start with the Hamiltonian of 2d electron gas in the presence of uniform magnetic field,

$$H = \frac{1}{2m}(-i\hbar\partial - e\mathbf{A})^2, \tag{E1}$$

with Landau gauge $\mathbf{A} = (-By, 0)$. We consider the cylinder geometry with periodic x direction. The energy levels (Landau level) are given by $\varepsilon_N = \hbar\omega_c(N + \frac{1}{2})$ where $\omega_c = |e|B/m$. The corresponding wave functions for the N-th Landau level are given by

$$\psi_{N,p_x}(x,y) \propto e^{ip_x x} e^{-(y-y_0)^2/2l^2} H_N(y - y_0), \tag{E2}$$

where $y_0 = \hbar p_x/eB$, l is the magnetic length, and H_N is the Hermite polynomial.

If we consider the boost deformation in x direction and impose the energy-twisted boundary condition, this amounts to shifting single-particle momentum, $p_x \to p_x + \lambda\varepsilon_N$. From the periodicity in x direction, $(p_x + \lambda\varepsilon_N)L = 2\pi r$ where r is an integer. As ε_N does not depend on p_x, this equation can be readily solved,

$$p_x = \frac{2\pi}{L}\left[r - \frac{L\lambda\varepsilon_N}{2\pi}\right]. \tag{E3}$$

As we change λ from 0 to $(2\pi)/(L\varepsilon_N)$, p_x changes from $2\pi r/L$ to $2\pi(r-1)/L$. This results in the shift of the Landau level center, $y_0 = (\hbar p_x)/(eB) = (\hbar 2\pi r)/(eBL) \to (\hbar 2\pi(r+1))/(eBL)$. As Laughlin's argument for the quantized Hall conductance, the adiabatic change in λ transports one electron ($\equiv 1N$) from one end of the cylinder to the other. Hence, $1N/1\lambda = 1/[(2\pi)/(L\varepsilon_N)] = (L\varepsilon_N)/(2\pi)$. The transported energy $1E = \varepsilon_N 1N$ is given by $(1E)/(1\lambda) = (L\varepsilon_N^2)/(2\pi)$. Following the analogy to Laughlin's argument for the quantized Hall conductance, the transverse energy transport is induced by the adiabatic insertion of a boost-analog of magnetic flux.

[1] J. M. Luttinger, Theory of thermal transport coefficients, Phys. Rev. **135**, A1505 (1964).

[2] W. Kohn, Theory of the insulating state, Phys. Rev. **133**, A171 (1964).

[3] J. T. Edwards and D. J. Thouless, Numerical studies of localization in disordered systems, J. Phys. C: Solid State Phys. **5**, 807 (1972).

[4] D. J. Thouless, Maximum Metallic Resistance in Thin Wires, Phys. Rev. Lett. **39**, 1167 (1977).

[5] R. Nakai, S. Ryu, and K. Nomura, Laughlin's argument for the quantized thermal hall effect, Phys. Rev. B **95**, 165405 (2017).

[6] S. Golkar and S. Sethi, Global anomalies and effective field theory, arXiv:1512.02607.

[7] M. Büttiker, Y. Imry, and R. Landauer, Josephson behavior in small normal one-dimensional rings, Phys. Lett. A **96**, 365 (1983).

[8] G. Rizzi and M. L. Ruggiero, eds., Relativity in rotating frames, 2004th ed., *Fundamental Theories of Physics* (Springer, New York, NY, 2003).

[9] K. Shiozaki, H. Shapourian, K. Gomi, and S. Ryu, Many-body topological invariants for fermionic short-range entangled topological phases protected by antiunitary symmetries, Phys. Rev. B **98**, 035151 (2018).

[10] H. Shapourian, K. Shiozaki, and S. Ryu, Many-Body Topological Invariants for Fermionic Symmetry-Protected Topological Phases, Phys. Rev. Lett. **118**, 216402 (2017).

[11] N. Trivedi and D. A. Browne, Mesoscopic ring in a magnetic field: Reactive and dissipative response, Phys. Rev. B **38**, 9581 (1988).

[12] D. J. Scalapino, S. R. White, and S. Zhang, Insulator, metal, or superconductor: The criteria, Phys. Rev. B **47**, 7995 (1993).

[13] T. Giamarchi and B. S. Shastry, Persistent currents in a one-dimensional ring for a disordered hubbard model, Phys. Rev. B **51**, 10915 (1995).

[14] B. S. Shastry, Sum rule for thermal conductivity and dynamical thermal transport coefficients in condensed matter, Phys. Rev. B **73**, 085117 (2006).

[15] R. Resta, Drude weight and superconducting weight, J. Phys.: Condens. Matter **30**, 414001 (2018).

[16] H. Castella, X. Zotos, and P. Prelovšek, Integrability and Ideal Conductance at Finite Temperatures, Phys. Rev. Lett. **74**, 972 (1995).

[17] X. Zotos, F. Naef, and P. Prelovsek, Transport and conservation laws, Phys. Rev. B **55**, 11029 (1997).

[18] S. Fujimoto and N. Kawakami, Exact drude weight for the one-dimensional hubbard model at finite temperatures, J. Phys. A: Math. Gen. **31**, 465 (1998).

[19] S. Mukerjee and B. S. Shastry, Signatures of diffusion and ballistic transport in the stiffness, dynamical correlation functions, and statistics of one-dimensional systems, Phys. Rev. B **77**, 245131 (2008).

[20] H.-H. Tu, Y. Zhang, and X.-L. Qi, Momentum polarization: An entanglement measure of topological spin and chiral central charge, Phys. Rev. B **88**, 195412 (2013).

[21] Y.-Z. You and M. Cheng, Measuring modular matrices by shearing lattices, arXiv:1502.03192 [cond-mat. str-el] (2015).

[22] Y. Yao and M. Oshikawa, Twisted Boundary Condition and Lieb-Schultz-Mattis Ingappability for Discrete Symmetries, Phys. Rev. Lett. **126**, 217201 (2021).

[23] Ö. M. Aksoy, A. Tiwari, and C. Mudry, Lieb-Schultz-Mattis type theorems for Majorana models with discrete symmetries, Phys. Rev. B **104**, 075146 (2021).

[24] T. Bargheer, N. Beisert, and F. Loebbert, Long-range deformations for integrable spin chains, J. Phys. A: Math. Theor. **42**, 285205 (2009).

[25] A. B. Zamolodchikov, Expectation value of composite field $T\bar{T}$ in two-dimensional quantum field theory, arXiv:hep-th/0401146.

[26] B. Pozsgay, Current operators in integrable spin chains: lessons from long range deformations, SciPost Physics **8**, 016 (2020).

[27] A. Klümper and K. Sakai, The thermal conductivity of the spin-$\frac{1}{2}$XXZ chain at arbitrary temperature, J. Phys. A: Math. Gen. **35**, 2173 (2002).

[28] J. V. Alvarez and C. Gros, Anomalous Thermal Conductivity of Frustrated Heisenberg Spin Chains and Ladders, Phys. Rev. Lett. **89**, 156603 (2002).

[29] F. Heidrich-Meisner, A. Honecker, D. C. Cabra, and W. Brenig, Thermal conductivity of anisotropic and frustrated spin-$\frac{1}{2}$ chains, Phys. Rev. B **66**, 140406(R) (2002).

[30] K. Saito, Transport anomaly in the low-energy regime of spin chains, Phys. Rev. B **67**, 064410 (2003).

[31] E. Orignac, R. Chitra, and R. Citro, Thermal transport in one-dimensional spin gap systems, Phys. Rev. B **67**, 134426 (2003).

[32] K. Sakai and A. Klümper, Non-dissipative thermal transport in the massive regimes of the XXZchain, J. Phys. A: Math. Gen. **36**, 11617 (2003).

[33] J. Cardy, Thermalization and Revivals after a Quantum Quench in Conformal Field Theory, Phys. Rev. Lett. **112**, 220401 (2014).

[34] T. D. Schultz, D. C. Mattis, and E. H. Lieb, Two-dimensional ising model as a soluble problem of many fermions, Rev. Mod. Phys. **36**, 856 (1964).

[35] P. Di Francesco, P. Mathieu, and D. Sénéchal, *Conformal Field Theory*, Graduate Texts in Contemporary Physics (Springer, New York, NY, 1997).

[36] L. D. Landau and E. M. Lifshitz, *Fluid Mechanics*, 2nd ed. (Butterworth-Heinemann, Oxford, England, 1987).

[37] H. Watanabe and M. Oshikawa, Quantum quench and f-sum rules on linear and non-linear conductivities, Phys. Rev. B **102**, 165137 (2020).

[38] H. Watanabe, Y. Liu, and M. Oshikawa, On the General Properties of Non-linear Optical Conductivities, J. Stat. Phys. **181**, 2050 (2020).

[39] Y. Tanikawa, K. Takasan, and H. Katsura, Exact results for nonlinear drude weights in the spin-$\frac{1}{2}$ xxz chain, Phys. Rev. B **103**, L201120 (2021).

[40] Y. Tanikawa and H. Katsura, Fine structure of the nonlinear drude weights in the spin-1/2 xxz chain, Phys. Rev. B **104**, 205116 (2021).

[41] K. Takasan, Y. Tanikawa, and H. Katsura (unpublished).

[42] A. Kapustin and L. Spodyneiko, Thermal Hall conductance and a relative topological invariant of gapped two-dimensional systems, Phys. Rev. B **101**, 045137 (2020).

[43] M. Suzuki, Relationship between d-dimensional quantal spin systems and (d+1)-dimensional ising systems: Equivalence, critical exponents and systematic approximants of the partition function and spin correlations, Prog. Theor. Phys. **56**, 1454 (1976).

[44] M. Suzuki, Transfer-matrix method and monte carlo simulation in quantum spin systems, Phys. Rev. B **31**, 2957 (1985).

[45] M. Suzuki and M. Inoue, The ST-Transformation approach to analytic solutions of quantum systems. I: General formulations and basic limit theorems, Prog. Theor. Phys. **78**, 787 (1987).

[46] B. Pirvu, V. Murg, J. I. Cirac, and F. Verstraete, Matrix product operator representations, New J. Phys. **12**, 025012 (2010).

[47] M. M. Rams, V. Zauner, M. Bal, J. Haegeman, and F. Verstraete, Truncating an exact matrix product state for the xy model: Transfer matrix and its renormalization, Phys. Rev. B **92**, 235150 (2015).

[48] L. P. Yang, Y. J. Wang, W. H. Xu, M. P. Qin, and T. Xiang, A quantum transfer matrix method for one-dimensional disordered electronic systems, J. Phys.: Condens. Matter **21**, 145407 (2009).